A new series of magnetic and luminescent layered hybrid materials obtained from thianthrene phosphonic acid: M(H 2 O)PO 3 -S 2 C 12 H 7 (M = Cu, Zn) and M(H 2 O) 2 (PO 2 OH-S 2 C 12 H 7) 2 (M = Mn, Co)

Geoffrey Letheux, Parameshwari Ganesan, Fabien Veillon, Julien Varignon, Olivier Pérez, Julien Cardin, Christophe Labbé, Guillaume Rogez, Mathilde Ligeour, Paul-Alain Jaffrès, et al.

A new series of magnetic and luminescent layered hybrid materials obtained from thianthrene phosphonic acid: $M(H_2O)PO_3$-$S_2C_{12}H_7$ (M = Cu, Zn) and $M(H_2O)_2(PO_2OH$-$S_2C_{12}H_7)_2$ (M = Mn, Co)

Geoffrey Letheux[a], Parameshwari Ganesan[b], Fabien Veillon[a], Julien Varignon[a], Olivier Perez[a], Julien Cardin[b], Christophe Labbé[b], Guillaume Rogez[c], Mathilde Ligeour[d], Paul-Alain Jaffrès[d] and Jean-Michel Rueff*[a]*

[a]Normandie Univ, ENSICAEN, UNICAEN, CNRS, CRISMAT, 6 Bd du Maréchal Juin, 14050 Caen Cedex, France.

[b]Normandie Univ, ENSICAEN, UNICAEN, CNRS, CIMAP, 6 Bd du Maréchal Juin, 14050 Caen Cedex, France.

[c]IPCMS, UMR Unistra-CNRS 7504, 23 rue du Lœss, BP 43, 67034, Strasbourg Cedex 2, France.

[d]Univ Brest, CEMCA UMR CNRS 6521, 6 Avenue Victor Le Gorgeu, 29238 Brest, France.

Keywords: Hybrid materials, metallophosphonate, layered structure, magnetism, luminescence.

*E-mail: jean-michel.rueff@ensicaen.fr

paul-alain.jaffres@univ-brest.fr

Summary

Four new metallophosphonates with the chemical formulas $M(H_2O)PO_3$-$S_2C_{12}H_7$ (M = Cu, Zn) and $M(H_2O)_2(PO_2OH$-$S_2C_{12}H_7)_2$ (M = Mn, Co) were synthesized using a hydrothermal route from the original bent rigid thianthrene-2-ylphosphonic acid (TPA). This organic precursor crystallizes in a non-centrosymmetric space group $P2_12_12_1$ and presents a unique bent geometry due to the presence of two sulfur atoms in its rigid platform architecture. Obtained as single crystal and polycrystalline powders, the structures of the four hybrid materials were solved from X-ray diffraction on single crystals in a monoclinic $P2_1/c$ space group. These compounds adopt a lamellar structure consisting of one inorganic subnetwork alternating with a 'sawtooth' double organic -$S_2C_{12}H_7$ subnetwork. The inorganic layers of these compounds are made of (PO_3C) or partially deprotonated (PO_2OHC) tetrahedra connected by the apices to isolated $ZnO_3(H_2O)$ tetrahedra, $Cu_2O_6(H_2O)_2$ copper dimers and cobalt and manganese $MO_4(H_2O)_2$ octahedra, where the latter two exhibit an isotype structure. Thermogravimetric analysis was performed to confirm the amount of water molecules present in the formula, to track the dehydration process of the structures, and to evaluate their thermal stability. The magnetic properties of the copper, cobalt, and manganese-based materials were investigated from 2K to 300K by using a SQUID magnetometer revealing dominant antiferromagnetic interactions with Weiss temperatures of -8.0, -10, and -1 K, respectively. These magnetic behaviors were further corroborated by first-principles simulations based on Density Functional Theory (DFT). Finally, the absorption and photoluminescence properties of both the ligand and hybrid materials were investigated, revealing diverse excitation and recombination mechanisms. The organic moiety based on thianthrene significantly influenced the absorption and emission, with additional peaks attributed to transition metals. Singlet and triplet states recombination were observed, accompanied by an unidentified quenching mechanism affecting the triplet state lifetime.

Introduction

Metal-Organic Frameworks (MOF) or coordination polymers are two terms [1] used to describe crystalline materials that were intensively studied over the past 20 years. These materials are typically synthesized under hydrothermal conditions, and one of the main

interests lies in their ability to adjust their structural features by selecting one metallic ion (homometallic materials[2]) or several (heterometallic materials[3,4]), as well as choosing one organic ligand or a combination of organic partners[5]. These possibilities offer a panel of structures (2D, 3D) and pave the way to a variety of properties (proton conduction,[6] multiferroic materials,[7,8,9] metal ion[10] or drug release[11]) which is a crucial first step towards applications (catalysis,[12] molecular magnets,[13] SHG-active materials, gas storage, and release,[14] bactericidal action,[15] gene delivery,[16,17]). The development of flexible frameworks[18] has resulted in "breathing materials"[19] or responsive materials (e.g. photo-responsive MOF[20]), which is an important feature in designing materials that respond to their environment. The flexibility of the framework can trigger the release of molecules (*e.g.* NO,[21] acetylene[22]). This flexibility can arise from variable metal-ligand coordination modes or the inherent flexibility of the ligand. In our previous works, we focused on utilizing phosphonic acid-based ligands due to their fascinating coordination properties.[23] In particular, we assessed the design of rigid phosphonic acids by directly placing/attaching this functional group to a carbon atom belonging to an aromatic (*e.g.* benzene,[24] fluorene,[25] tetraphenylmethane[26]) or heteroaromatic moiety (thiophene[27]). Consequently, we found that the topology of the resulting hybrid materials was dictated, or at least influenced, by this rigidity of the organic ligand. Building on this concept, we employed rigid phosphonic acids with a low symmetry and discovered that in a couple of cases, these precursors produced non-centrosymmetric materials[9] and, in a few cases, homochiral materials[2]. To further explore materials with novel properties and potential dynamic conformations, we became interested in incorporating the thianthrene heterocycle (**Figure 1A**) into the structure of crystalline hybrid materials. It is worth noting that thianthrene is well-known for its luminescent properties[28] (fluorescence and phosphorescence), exhibits thermal stability as recently illustrated with polymers containing thianthrene [29], and possesses a remarkable flexible boat-type conformation. Numerous studies have revealed interesting photoluminescence properties in thianthrene derivatives, including strong Room Temperature Phosphorescence (RTP) [30,31], Aggregation-Induced/Enhanced emission [32], Thermally Activated Delayed Fluorescence[33], the coexistence of fluorescence and phosphorescence at room temperature [34,35]. This dual luminescence arises from recombination of singlet and triplet states and is modulated by spin-orbit coupling (SOC) between the lone pair electron of p-orbital of the sulfur atoms and the p-orbital of the

phenyl ring. The SOC is induced by the folding of the thianthrene molecule along the S—S axis.[33] Both the intersystem crossing (ISC) and the reverse intersystem crossing (RISC) depend on the folding-induced spin-orbit coupling (SOC), resulting in an increased phosphorescence/fluorescence intensity ratio and modification of transition rates as the folding angle decreases. Depending on the SOC strength, transitions occur from the S_1 state to the triplet manifold (T_n, n=1-6) state with the more favorable energy gap resulting in molecular electronic transitions of type π-π* and n-π*. Additionally, the reduction of non-radiative recombination channels in thianthrene-based materials due to their rigid environment significantly contributes to the presence of luminescence from both singlet and triplet states at room temperature. Moreover, this molecule shows ring inversion dynamics (through a pseudo-planar structure) with a remarkably low energy barrier (estimation: 5.5 $kcal.mol^{-1}$[36]). Furthermore, functionalizing thianthrene with one phosphonic acid (depicted in **Figure 2** as thianthrene-phosphonic acid, TPA) breaks the symmetry of the molecule and results in a chiral molecule that racemizes at room temperature due to rapid inversion dynamics (**Figure 1B**). The incorporation of thianthrene into hybrid materials could potentially affect the inversion dynamics, leading to the formation of either centrosymmetric or non-centrosymmetric materials, including homochiral materials by producing racemic conglomerates. In this study, we report the first synthesis of thianthrene functionalized with one phosphonic acid and demonstrate its utility in the synthesis of Zn, Cu, Co, or Mn-based crystalline hybrid materials. The report includes a comprehensive characterization of the resulting materials, encompassing their structure, thermal stability, magnetic properties, Density Functional Theory (DFT) and luminescent properties.

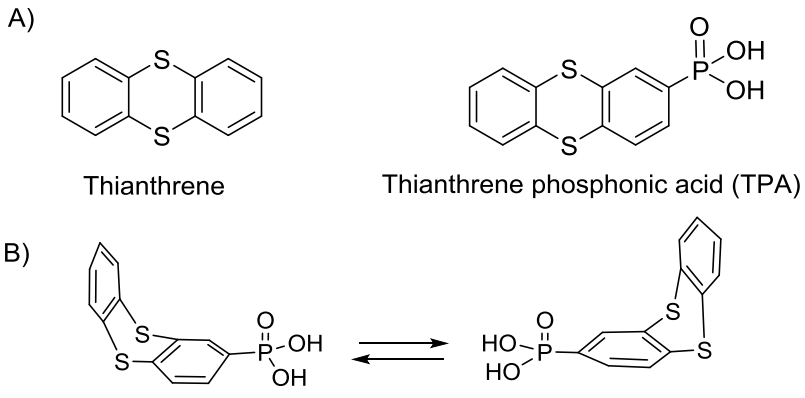

Figure 1 : A) Structure of thianthrene and thianthrene phosphonic acid (TPA) reported in this study; B) Schematic representation of conformation dynamics of TPA and its chiral trend.

Experimental

All reagents were used as received and without further purification. ^{1}H, ^{31}P and ^{13}C NMR were recorded on Bruker Avance DRX 500 spectrometers. Mass spectrometry was recorded on Bruker Autoflex MALDI TOF-TOF III. Zinc chloride ($ZnCl_2$, ≥98%), copper nitrate trihydrate ($Cu(NO_3)_2.3H_2O$, ≥99%), cobalt chloride hexahydrate ($CoCl_2.6H_2O$, ≥98%), and manganese chloride tetrahydrate ($MnCl_2.4H_2O$, ≥98%), were purchased from Sigma Aldrich and Alfa Aesar. Thianthrene-2-ylphosphonic acid (**3**) was prepared by adapting the reported methods described below. Hydrothermal syntheses were realized by using a Berghof digestec DAB-2 pressure digestion vessels. Elemental analyses were performed with an automatic CHNS-O ThermoFisher Flash 2000 instrument. Thermogravimetric analyses (TGA) were realized in alumina crucibles under reconstructed air stream (80% N_2/20% O_2 in volume) at the rate of 3°C/min from room temperature to 1000°C on polycrystalline samples by using a SETARAM Setsys Evolution apparatus. Each hybrid thermogram was systematically corrected by subtraction of the thermal behavior curve of the empty alumina crucible. Magnetic measurements were carried out using a squid magnetometer (Magnetic Properties Measurement System-XL-5T, Quantum Design). Magnetization was recorded under 1000 Oe by heating from 2 K to 300 K in settle mode after zero field (ZFC) and field cooling (FC). Powder samples were inserted into a gelatin capsule and then placed in a plastic straw. Selection of single crystals platelets and needles for single-crystal X-ray diffraction were performed using a polarizing Zeiss discovery V20 stereo-microscope. Data collection is performed on a Synergy S Rigaku diffractometer equipped with an Eiger 1M Dectric photon counting detector and Cu microfocus X-ray source; data reduction is done using Crysalispro. The crystal structure of compounds was solved with Olex 2[37] software. H atoms are positioned geometrically and refined using a riding model. Powders X-ray diffraction patterns were recorded with a laboratory X-Pert Pro Panalytical diffractometer with Cu Kα1/Kα2 radiation ($\lambda K_{\alpha 1}$ = 1.540598 Å and $\lambda K_{\alpha 2}$= 1.544426 Å) equipped with PIXcel detector. The absorbance spectra were measured using a PerkinElmer LAMBDA 1050+ UV/Vis/NIR spectrophotometer with 150 mm integrating sphere in total transmittance mode at normal incidence. Absorbance (A) values were calculated from the transmittance measurements. The samples were prepared as powder stacked between two Suprasil glass slides [Hellma

Analytics]. Gaussian functions were employed to fit the absorbance spectra and determine the positions of the bands. For continuous Wavelength (CW) Photoluminescence (PL) measurements, a continuous wave laser (Crylas FQCW266) with an excitation wavelength of 266 nm was used. The measurements were conducted at room temperature with an average power of 26 mW/mm^2, and the chopper frequency was set to 15 Hz. Photon collection and dispersion were performed using a Horiba Triax 180 monochromator equipped with a 600 grooves per mm grating blazed at 1 µm. A Hamamatsu photomultiplier tube connected to a FEMTO DLPCA-200 trans-impedance amplifier was used for photon detection. The amplified signal was directed to a lock-in amplifier, synchronized with the chopper controller's reference frequency. Two PL measurements were conducted for each sample. The first measurement covered the range from 4.13 to 2.06 eV (300 to 600 nm) without any filter or using long pass filter 300 (FEL300, Edmund Optics-colored glass filter). The second measurement encompassed the range from 3.09 to 1.38 eV (400 to 900 nm) employing different long-pass filters specific to each compound. These filters had cut-on wavelengths at 400 nm, 450 nm, and 600 nm, (Thorlabs FEL 400, FEL 450, FEL 600). Gaussian functions were employed to fit PL spectra and identify the bands' positions.

Photoluminescence decay time curves were measured using a custom-built time-resolved setup. A NT340 EKSPLA Optical Parametric Oscillator (OPO) was used as a tunable source, generating pulse linewidths at 266 nm of almost 5 ns much lower than the measured decay times. The repetition rate of the OPO was adjustable up to 10 Hz. For wavelength selection and detection in photoluminescence, an HR320 monochromator and a C31034 photomultiplier tube (PMT) detector were employed. The data acquisition was performed using a Teledyne Lecroy HDO4032 oscilloscope, and the data were recorded on a computer using a Labview program developed in-house. The photoluminescence signal was detected at room temperature through a set of long-pass filters (300 nm, 400 nm, 500 nm, 600 nm) depending on the selected detection wavelengths. The time variation of the photoluminescence intensity at each selected wavelength was calculated using a mean decay time (τ_m) model given by the following formula:

$$<\tau_m> = \frac{\int_0^\infty \boldsymbol{I_{PL}(t)dt}}{\boldsymbol{I_0}}$$

where $I_{PL}(t)$ is the PL decay time intensity and I_0 is the maximum PL intensity at t=0.

First-principles simulations are performed using Density Functional Theory (DFT) as implemented in the Vienna Ab initio Simulation Package (VASP) package[38,39]. Projector Augmented Wave (PAW)[40] have been used for modelling the core electrons and only the outer d electrons and s electrons are treated for Cu, Mn and Co (4s3d). Experimental structures are used as the input geometry for the simulations. The energy cut-off is set to 500 eV and the convergence of the total energy is fixed to 10^{-7} eV between consecutive self consistent steps. The Brillouin zone is sampled by a 3x8x4, 3x8x8 and 4x8x3 kmesh for compounds based on Mn, Cu and Co, respectively. Two exchange-correlation fucntionals are used: the Perdew-Burke-Ernzherof Generalized Gradient Approximation (GGA) revised for solids (PBEsol)[41] and the meta-GGA Strongly Constrained and Appropriety Normalized (SCAN) functional[42].

Synthesis

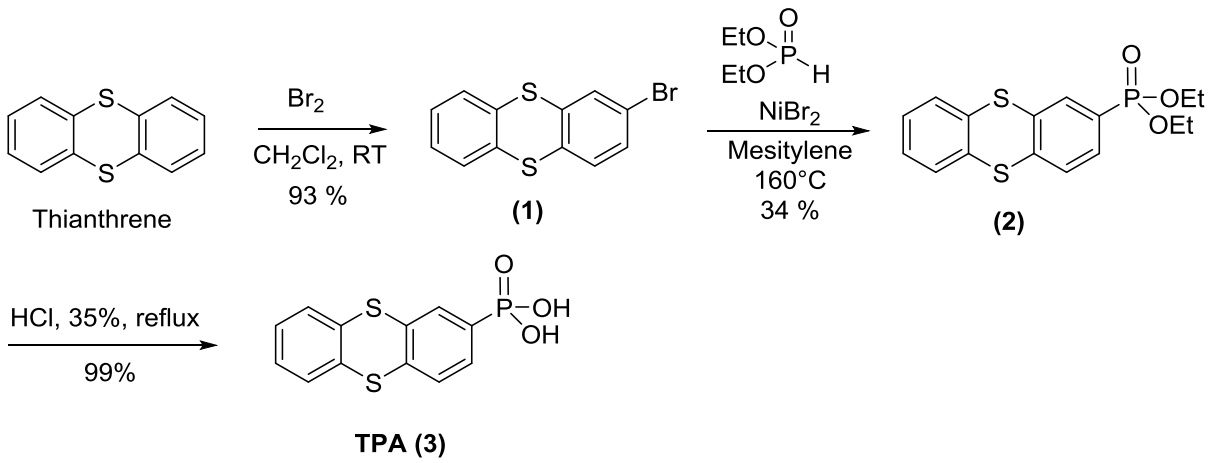

Figure 2 : Synthesis of thianthrene phosphonic acid (**(3)** TPA)

Synthesis of 2-bromothianthrene (1):

Bromine (6.65 g, 41.6 mmol; 0.9 eq) was slowly added to a solution of thianthrene (10 g, 46.3 mmol; 1 eq) in dichloromethane (150 mL) under nitrogen. The mixture was stirred 24 hours at 25°C. The solution was washed with $NaHSO_3$ (0.5 M aqueous solution, 100 mL) to quench the residual bromine, and then with water (2*100 mL). The organic solution was dried over $MgSO_4$, filtered, and concentrated to produce 11.54 g of white solid. This compound, that presents some impurities, was used in the subsequent step without further

purification. Its spectroscopic (^{1}H) characteristics are consistent with those from the literature [43,44].

Synthesis of 2-Diethylphosphonothianthrene (2):

Triethyl phosphite (6.7 g, 41 mmol) was added dropwise, and carefully to a reflux solution of 2-bromothianthrene (11.54 g) and nickel (II) bromide (0.4 g, 1.6 mmol) in mesitylene (20 mL). After the addition, the mixture was stirred and heated for 6 hours. Mesitylene was partly distilled under vacuum. Dichloromethane (150 mL) and water (150 mL) were added. This solution was slowly stirred overnight. The organic layer was washed with water (100 mL) and dried over $MgSO_4$. After filtration and concentration, the resulting solid (11.48 g) was purified by two successive column chromatography on silica gel (DCM/MeOH 100/0.5 to 100/2.5 in volume). The fraction of chromatography corresponding to the product was placed in a Kugelrohr to remove volatile impurities (140°C, 3.10^{-2} mbar for 2h). 2-diethylphosphonothianthrene **(2)** was obtained as a viscous oil (4.8 g, 34 % from thianthrene, two steps). Rf = 0.57 (DCM/ MeOH 95: 5); 1H-NMR (500 MHz, 20 °C, CDCl3, δ): 1.30 (t, 3JHH = 7.1 Hz, 6H), 4.02-4.15 (m, 4H), 7.24-7.26 (m, 2H), 7.44-7.47 (m, 2H), 7.54 (dd, 3JHH = 7.9 Hz, 4JHP = 4.0 Hz ,1H), 7.63 (ddd, 3JHP = 12.7 Hz, 3JHH = 7.9 Hz , 4JHH = 1.3 Hz , 1H), 7.87 (dd, 3JHP = 13.3 Hz, 4JHH = 1.3 Hz, 1H); 31P{1H}-NMR (202.4 MHz, 20 °C, CDCl3, δ): 17.8 ; 13C{1H}-NMR (125.7 MHz, 20 °C, CDCl3, δ) : 16.35 (d, 3JCP = 6.3 Hz), 62.35 (d, 2JCP = 6.0 Hz), 128.1 (d, 1JCP = 189.0 Hz, C), 130.74 (s, CH), 130.81 (s, CH), 131.29 (d, 3JCP = 15.9 Hz, CH), 131.47 (s, CH), 131.56 (s, CH), 133.44 (d, 2JCP = 10.0 Hz, CH), 134.35 (d, 2JCP = 11.1 Hz, CH), 137.10 (s, C), 137.41 (s, C), 138.79 (d, 3JCP = 17.5 Hz, C), 143.75 (d, 4JCP = 2.8Hz, C). mass (MALDI-TOF; matrix dithranol): m/z calcd for C16H17O3PS2Na [M+Na]+: 375.025, found 375.124; m/z calcd for C16H17O3PS2K [M+K]+: 390.999, found 391.105.

Synthesis of thianthrene-2-ylphosphonic acid (3 ; TPA):

2-Diethylphosphonothianthrene (2.6 g, 7.38 mmol) and concentrated HCl solution (37% in water, 120 mL) were heated at reflux overnight. Water and the excess of HCl were removed in a vacuum. The last traces of water were removed by azeotropic distillation with toluene. Thianthrene-2-ylphosphonic acid was obtained as a white solid (2.18 g, 99.5%).

m.p. 125 °C; ^{1}H-NMR (500 MHz, CD_3OD, 20 °C, δ): 7.29-7.31(m, 2H), 7.48-7.50 (m, 2H), 7.58 (dd,$^3J_{HH}$ = 7.9 Hz, $^4J_{HP}$ = 3.7 Hz, 1H), 7.66 (ddd, $^3J_{HP}$ = 15.6 Hz, $^3J_{HH}$ = 7.9 Hz, $^4_{JHH}$ = 1.2 Hz, 1H),

7.85 (dd,$^{3}J_{HP}$ = 13.4 Hz, $^{4}J_{HH}$ = 1.2 Hz, 1H)**;** ^{31}P {^{1}H}-NMR (202.4 MHz, CD_3OD, 20 °C, δ): 15.6 **;** ^{13}C {^{1}H}-NMR (125.7 MHz, CD_3OD, 20 °C, δ): 129.27 (s, CH), 129.32 (s, CH), 129.50 (d, CH), 129.70 (s, CH), 129.75 (s, CH), 131.17 (d, $^{2}J_{CP}$ = 10.2 Hz, CH), 161.5 (d, $^{2}J_{CP}$ = 11.4 Hz, CH), 132.24 -d, $^{1}J_{CP}$ = 186.3 Hz, C), 135.82 (s, C), 132.60 (s, C), 137.07 (d, $^{3}J_{CP}$ = 17.3 Hz, C), 141.23 (s broad, CH).

Crystals of thianthrene phosphonic acid (TPA) were isolated after a slow evaporation of a solution of TPA in methanol.

Synthesis of the hybrid materials

All hybrid materials were initially synthesized by hydrothermal method, which is an adapted technique to obtain single crystals. These crystals were then used for the detailed structural analysis of the materials. After carefully selecting the crystals, we assessed the overall purity of the batches using X-ray powder diffraction and Le Bail [45] refinements based on the CIF file acquired from X-ray diffraction on single crystal resolution. This method allowed to confirm the purity and homogeneity of the zinc and copper and unveiled the presence of an unidentified second phase in the cobalt and manganese compounds. Subsequently, we conducted a soft chemistry synthesis to obtain pure phases of the cobalt and manganese compounds, whose structure was solved following the meticulous selection of single crystals **(FIGURE SI 1)** from the biphasic batch obtained through hydrothermal synthesis.

Hydrothermal synthesis

$Zn(H_2O)(PO_3S_2C_{12}H_7)$ (4):

A mixture of thianthrene-2-ylphosphonic acid $C_{12}PS_2O_3H_9$ (0.03 g, 0.10 mmol, 1 eq.), zinc chloride $ZnCl_2$ (0.014 g, 0.10 mmol, 1 eq.), urea CH_4N_2O (0.006 g, 0.10 mmol, 1 eq.) and distilled water (10 mL) was inserted in a 50 mL PTFE liner. After closing, the liner is charged in a Digestec Berghof DAB-2 pressure vessel and heated from room temperature to 130°C in 20 hours, left at 130°C for 20 hours, and cooled to room temperature in 24 hours. After filtration, the final material obtained as white needles polycrystalline sample is firstly washed with water and secondly with ethanol before being left in the air to dry (quantity 21 mg; yield 55 %.).

Elemental analysis for $ZnPS_2C_{12}O_4H_9$ (377.69 g/mol): found (calc.) C 38.54% (38.16 %), H 2.26% (2.40 %), S 16.50% (16.98 %).

$Cu(H_2O)(PO_3S_2C_{12}H_7)$ (5):

A mixture of thianthrene-2-ylphosphonic acid $C_{12}PS_2O_3H_9$ (0.03 g, 0.10 mmol, 1 eq.), copper nitrate trihydrate (0.024 g, 0.10 mmol, 1 eq.), urea CH_4N_2O (0.006 g, 0.10 mmol, 1 eq.) and distilled water (10 mL) was inserted in a 50 mL PTFE liner. After closing, the liner is charged in a Digestec Berghof DAB-2 pressure vessel and heated from room temperature to 140°C in 10 hours, left at 140°C for 36 hours, and cooled to room temperature in 10 hours. After filtration, the final material obtained as green platelets polycrystalline sample is firstly washed with water and secondly with ethanol before being left in the air to dry (quantity 27 mg; yield 71 %).

Elemental analysis for $CuPS_2C_{12}O_4H_9$ (375.85 g/mol): found (calc.) C 38.88% (38.35 %), H 2.21% (2.41 %), S 17.08% (17.07 %).

$Co(H_2O)_2(PO_2OHS_2C_{12}H_7)_2$ (6):

A mixture of thianthrene-2-ylphosphonic acid $C_{12}PS_2O_3H_9$ (0.03 g, 0.10 mmol, 1 eq.), cobalt chloride hexahydrate (0.024 g, 0.10 mmol, 1 eq.), urea CH_4N_2O (0.006 g, 0.10 mmol, 1 eq.) and distilled water (10 mL) was inserted in a 50 mL PTFE liner. After closing, the liner is charged in a Digestec Berghof DAB-2 pressure vessel and heated from room temperature to 160°C in 20 hours, left at 160°C for 20 hours, and cooled to room temperature in 24 hours. After filtration, the final material obtained as pink platelets polycrystalline sample is firstly washed with water and secondly with ethanol before being left in the air to dry.

$Mn(H_2O)_2(PO_2OHS_2C_{12}H_7)_2$ (7):

A mixture of thianthrene-2-ylphosphonic acid $C_{12}PS_2O_3H_9$ (0.03 g, 0.10 mmol, 1 eq.), manganese chloride tetrahydrate (0.02 g, 0.10 mmol, 1 eq.), urea CH_4N_2O (0.006 g, 0.10 mmol, 1 eq.) and distilled water (10 mL) was inserted in a 50 mL PTFE liner. After closing, the liner is charged in a Digestec Berghof DAB-2 pressure vessel and heated from room temperature to 160°C in 20 hours, left at 160°C for 20 hours, and cooled to room temperature in 24 hours. After filtration, the final material obtained as white platelets polycrystalline sample is firstly washed with water and secondly with ethanol before being left in the air to dry.

Soft chemistry synthesis of $Co(H_2O)_2(PO_2OHS_2C_{12}H_7)_2$ (6) and $Mn(H_2O)_2(PO_2OHS_2C_{12}H_7)_2$ (7)

$Co(H_2O)_2(PO_2OHS_2C_{12}H_7)_2$ (6):

In a 100 mL round bottom flask a mixture of thianthrene-2-ylphosphonic acid $C_{12}PS_2O_3H_9$ (0.05 g, 0.17 mmol, 1 eq.) and urea CH_4N_2O (0.010 g, 0.17 mmol, 1 eq.) was dissolved in 30 mL of demineralized water heated a set point of 120°C. A water solution (20 mL) of cobalt chloride hexahydrate $CoCl_2.6H_2O$ (0.02 g, 0.08 mmol, 0.5eq.) was slowly added to the previous mixture solution. The pink formed precipitate was stirred for 4 hours at reflux of the solvent and cooled to room temperature in 12 hours. After filtration, the final material obtained as the pink powder was first washed with water and secondly with ethanol before being left to dry in the air (final quantity 29 mg; yield 50%).
Elemental analysis for $CoP_2O_8S_4C_{24}H_{20}$ (685.55 g/mol): found (calc.) C 41.96% (42.05 %), H 3.02% (2.66 %), S 18.85% (18.76%).

$Mn(H_2O)_2(PO_2OHS_2C_{12}H_7)_2$ (7):

In a 100 mL round bottom flask a mixture of thianthrene-2-ylphosphonic acid $C_{12}PS_2O_3H_9$ (0.05 g, 0.17 mmol, 1 eq.) and urea CH_4N_2O (0.010 g, 0.17 mmol, 1 eq.) was dissolved in 30 mL of demineralized water heated at a set point of 120°C. A water solution (20 mL) of manganese chloride tetrahydrate $MnCl_2.4H_2O$ (0.017 g, 0.08 mmol, 0.5eq.) was slowly added to the previous mixture solution. The light brown formed precipitate was stirred for 4 hours at reflux of the solvent and cooled to room temperature in 12 hours. After filtration, the final material obtained as the slightly brown powder was first washed with water and secondly with ethanol before being left to dry in the air (final quantity 24 mg; yield 42%).
Elemental analysis for $MnP_2O_8S_4C_{24}H_{20}$ (681.56 g/mol): found (calc.) C 42.54% (42.42 %), H 2.96% (2.68 %), S 17.70% (18.82%).

Thermogravimetric analysis

The thermogravimetric analysis of $Zn(H_2O)(PO_3S_2C_{12}H_7)$ **(4)** and $Cu(H_2O)(PO_3S_2C_{12}H_7)$ **(5)** $Co(H_2O)_2(PO_2OHS_2C_{12}H_7)_2$ **(6)** and $Mn(H_2O)_2(PO_2OHS_2C_{12}H_7)_2$ **(7)** were performed on polycrystalline powder samples from room temperature to 1000°C at the rate of 3°C/min

under a synthetic air atmosphere (mixture of 20% of O_2 and 80% of N_2 in volume). The TGA curves of the four compounds are presented **Figure 3 a-b**. The four curves present a first weight loss of -4.71 % from 115°C to 290°C **(4)**, -5.19 % from 90°C to 220°C **(5)**, -5.35% from 100°C to 150°C **(6)** and -5.26 % from 90°C to 141 °C **(7)** respectively which is in good agreement with the value expected for the departure of the water molecule present in the formula of each compound (calculated: -4.76% **(4)**, -4.79% **(5)** -5.25 % **(6)**, -5.28% **(7)**). For the cobalt and manganese hybrids **(Figure 3 b)**, a second loss of mass of -2.41% **(6)** and -2.87% **(7)** is observed up to 250°C. After this dehydration process, a plateau is seen reflecting the thermal stability of the compounds up to 320°C **(5)** and 380°C **(4, 6, 7)** followed by a new weight loss associated to the decomposition of the organic moiety. At 1000°C, the final weight losses of -60.48% **(4)**, -62.43% **(5)** -70.74% **(6)**, -70.57% **(7)** are in good agreement with the values expected for the formation of $Zn_2P_2O_7$ (calculated -59.66%), $Cu_2P_2O_7$ (calculated -59.95%), CoP_2O_6 (calculated -68.4%), MnP_2O_6 (calculated -68.8%). The formation of these pyrophosphates was confirmed by X-ray diffraction performed on the thermal decomposition products for **(4)**, **(5)**, **(6)** and a mixture of $Mn_2P_2O_7$ and MnP_2O_6 **(7)(FIGURE SI 2)**.

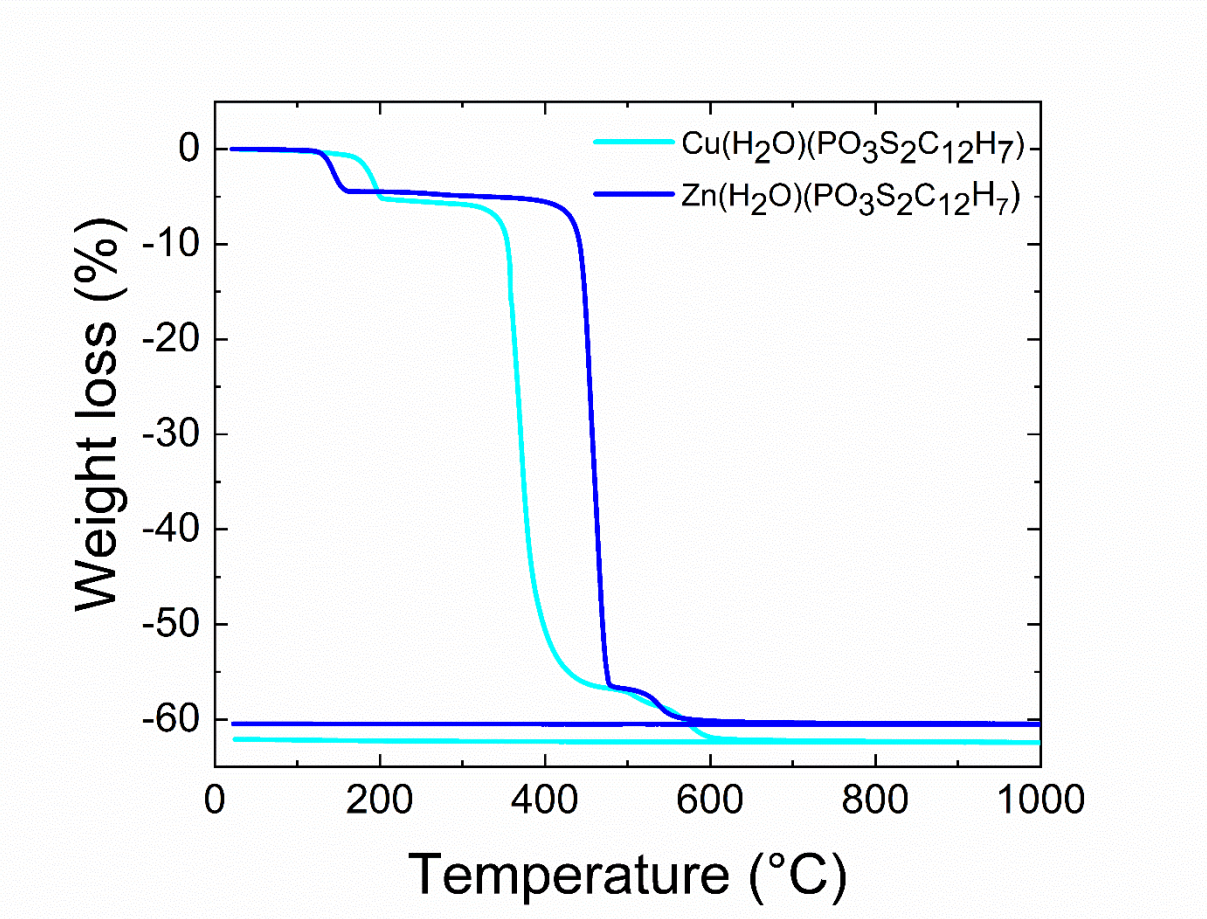
Cu(H2O)(PO3S2C12H7)
Zn(H2O)(PO3S2C12H7)
Weight loss (%)
0
-10
-20
-30
-40
-50
-60
0
200
400
600
800
1000
Temperature (°C)

(a)

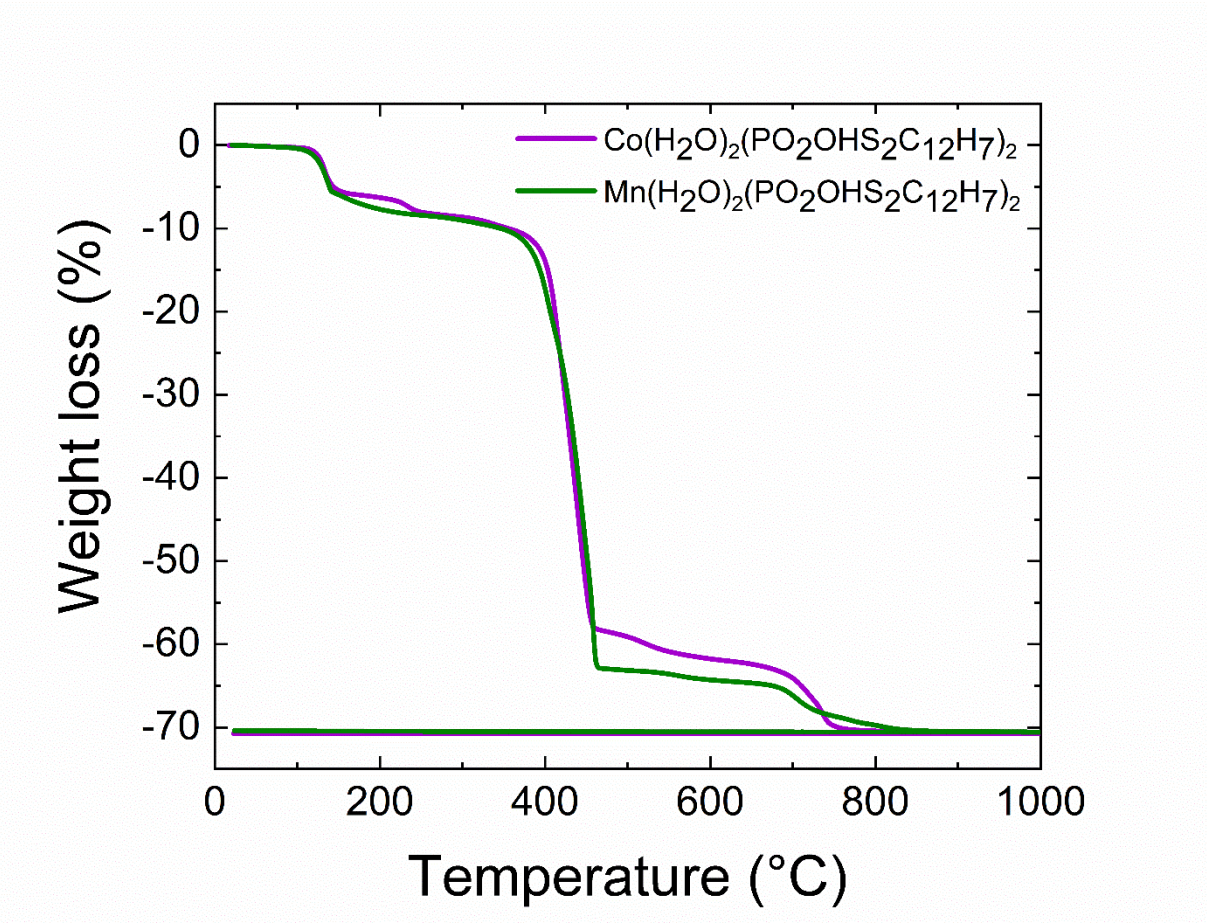

(b)

Figure 3 : Thermogravimetric curves of the compounds (a) $Zn(H_2O)(PO_3S_2C_{12}H_7)$ **(4)** and $Cu(H_2O)(PO_3S_2C_{12}H_7)$ **(5)**; (b) $Co(H_2O)_2(PO_2OHS_2C_{12}H_7)_2$ **(6)** and $Mn(H_2O)_2(PO_2OHS_2C_{12}H_7)_2$ **(7)** recorded under an air atmosphere at the rate of 3°C/min.

Structural Description from X-ray Diffraction on Single Crystal

The crystallographic data for $PO(OH)_2S_2C_{12}H_9$ **(3)**, $Zn(H_2O)(PO_3S_2C_{12}H_7)$ **(4)**, $Cu(H_2O)(PO_3C_{12}S_2H_7)$ (**5**), $Co(H_2O)_2(PO_2OHS_2C_{12}H_7)_2$ **(6)** and $Mn(H_2O)_2(PO_2OHS_2C_{12}H_7)_2$ **(7)** obtained from single-crystal X-ray diffraction study are reported **Table 1.**

Table 1: Crystallographic Data for $PO(OH)_2S_2C_{12}H_9$ **(3)**, $Zn(H_2O)(PO_3S_2C_{12}H_7)$ **(4)**, $Cu(H_2O)(PO_3C_{12}S_2H_7)$ **(5)**, $Co(H_2O)_2(PO_2OHS_2C_{12}H_7)_2$ **(6)** and $Mn(H_2O)_2(PO_2OHS_2C_{12}H_7)_2$ **(7)** from single crystal X-ray diffraction study

Formula	**$PO(OH)_2S_2C_{12}H_7$**	**$Zn(H_2O)(PO_3S_2C_{12}H_7)$**	**$Cu(H_2O)(PO_3S_2C_{12}H_7)$**	**$Co(H_2O)_2(PO_2OHS_2C_{12}H_7)_2$**	**$Mn(H_2O)_2(PO_2OHS_2C_{12}H_7)_2$**
Compound number	**3**	**4**	**5**	**6**	**7**
Molecular formula	$PO_3S_2C_{12}H_9$	$ZnPO_4S_2C_{12}H_9$	$CuPO_4S_2C_{12}H_9$	$CoP_2O_8S_4C_{24}H_{20}$	$MnP_2O_8S_4C_{24}H_{20}$
Molecular weight (g mol^{-1})	296.30	377.69	375.85	685.55	681.56
Space group	$P2_12_12_1$	$P2_1/c$	$P2_1/c$	$P2_1/c$	$P2_1/c$
a (Å)	4.80963 (5)	22.0947 (5)	22.0156 (5)	22.1542 (2)	22.20022 (9)
b (Å)	10.61773 (11)	7.8428 (2)	7.6616 (2)	7.93590 (10)	8.01328 (3)
c (Å)	24.017 (2)	7.8758 (2)	7.5811 (2)	15.1100 (2)	15.22699 (7)
α (°)	90	90	90	90	90
β (°)	90	95.283 (2)	95.297 (2)	93.846 (10)	93.8226 (4)
γ (°)	90	90	90	90	90
Z	4	4	4	4	4
V ($Å^3$)	1226.48 (2)	1358.96 (6)	1273.28 (6)	2650.56 (5)	2702.90 (2)
$d_{calc.}$ [g/cm^3]	1.605	1.846	1.961	1.718	1.675
μ [mm^{-1}]	5.158	6.596	6.783	9.604	8.412
Radiation source λ [Å]	Cu Kα 1.54184	Cu Kα 1.54184	Cu Kα 1.54184	Cu Kα 1.54184	Cu Kα 1.54184
θ range [°]	3.65-75.53	4.04-75.257	4.055-73.549	3.99-75.609	3.958-75.628
No. of independent reflections with $I \geq 2\sigma(I)$	23440	27137	21112	28423	186132

Number of refined parameters	166	186	186	363	364
Weighted R factor (%)	6.60	12.83	16.59	21.95	7.91
$R[F^2 > 2\sigma(F^2)]$ (%)	2.44	3.72	6.08	7.13	3.07
R_{int} (internal R value) (%)	3.59	7.97	8.10	3.83	4.77
S (goodness of the fit)	1.047	1.006	1.116	1.199	1.148

The thianthrene-2-ylphosphonic acid of formula $PO(OH)_2S_2C_{12}H_7$ **(3)** crystallized in a non-centrosymmetric $P2_12_12_1$ orthorhombic space group with the parameters a=4.80963(5) Å, b=10.61773(11) Å, c=24.0170(2) Å, and V=1226.48(2) $Å^3$. The absence of water molecules in the structure was confirmed by thermogravimetric analysis **(FIGURE SI 3)**. The crystal structure is made of layers regularly stacked along the *b* direction and shifted to 1/2 along to the *c* direction. The P-O distances (d_{P-O}) of the phosphonic function vary from 1.4923(18) Å to 1.5536(18) Å and the P-C distance (d_{P-C}) is equal to 1.782(3) Å. In one layer, the $PO(OH)_2S_2C_{12}H_7$ molecules are connected through the fully protonated phosphonic function $PCO(OH)_2$ by a zigzag network of hydrogen bonds, with O•••H-O distances ranging from 1.7999(17) Å to 3.2623(17) Å **(Figure 4a)**, and organized in supramolecular columns running along the *a* direction **(Figure 4b)**. Two adjacent columns are connected by C•••H-C interactions arising from the C_6H_4 rings, with distances varying from 2.813(4) Å to 3.160(4) Å. Inside one supramolecular column, the smallest S•••H-C distance was evaluated to 3.6352(8) Å. The cohesion of the structure is ensured by a network of C•••H-C and S•••H-C interactions connecting the layers together. The C•••H-C and S•••H-C distances are respectively ranging from 2.709(4) Å to 3.285(3) Å and 2.9836(8) Å to 3.2007(8) Å in good agreement with the values described in the literature[46] **(Table SI 1)**. Finally, the value of the folding angle, equal to 132.7(5)°, was determined by evaluating the angles between the planes passing through the atoms (C3, C8, S2, S9) and (C1, C10, S2, S9) **(FIGURE SI 4)**. This value, close to the theoretical one of 128°,[47] will be compared to the one found in the structure of the hybrid-based material (**4**, **5**, **6,** and **7**) to evaluate the influence of their structure on the constraints and deformation of this bent molecule.

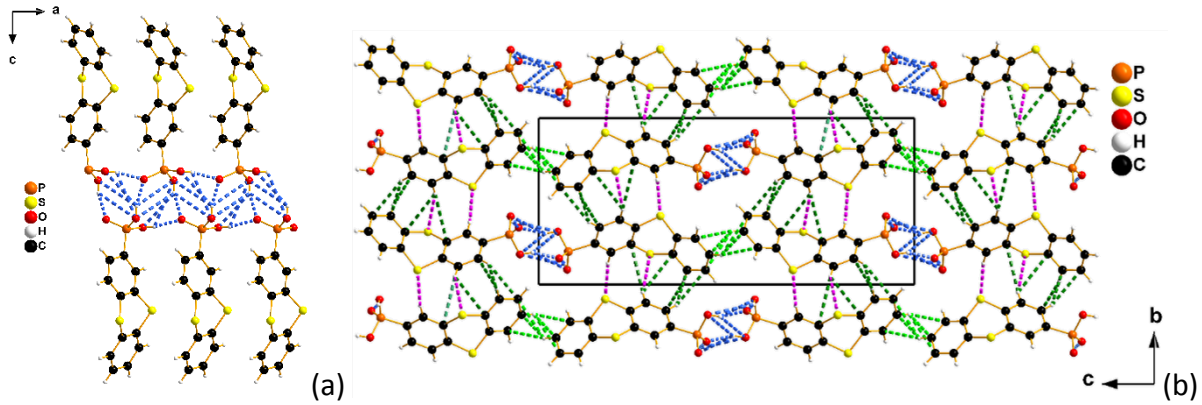

Figure 4 : (a) Zigzag network of hydrogen bonds, with O•••H-O distances ranging from 1.7999(17) Å to 3.2623(17) Å. (b) Structure of phosphonic acid of formula $PO(OH)_2S_2C_{12}H_7$

viewed along the *a* direction. The blue dashed lines represent the intermolecular O•••H-O hydrogen bonds between the phosphonic acid functions; the green dashed lines represent the intermolecular C•••H-C interaction between the C_6H_4 rings and two layers; the pink dashed lines represent the intermolecular S•••H-C interaction between two layers.

The four hybrid materials $Zn(H_2O)(PO_3S_2C_{12}H_7)$ **(4)**, $Cu(H_2O)(PO_3S_2C_{12}H_7)$ **(5)**, $Co(H_2O)_2(PO_2OHS_2C_{12}H_7)_2$ **(6)** and $Mn(H_2O)_2(PO_2OHS_2C_{12}H_7)_2$ **(7)** were obtained by hydrothermal synthesis as single crystals and pure polycrystalline phases as presented **Figure SI 1** for pattern matching of the phase from CIF file from thianthrene-2-ylphosphonic acid and the corresponding metal transition salt. Their structures were solved by X-ray diffraction on single crystals. These compounds present the similar feature of crystallizing in a lamellar structure made of a regular stacking of one inorganic layer alternating with one double organic layer along the *a* direction **(Figure 5)** (see Figure SI 5 for (**7**)). These four compounds crystallized in a centrosymmetric P21/c monoclinic space group with the following fairly close parameters a=22.0947(5) Å, b=7.8428(2) Å, c=7.8758(2) Å, β=95.283(2)°, V=1358.96(6) $Å^3$ for $Zn(H_2O)(PO_3S_2C_{12}H_7)$ **(4)**; a=22.0156(5) Å, b=7.6616(2) Å, c=7.5811(2) Å, β=95.297(2)°, V=1273.28(6) $Å^3$ for $Cu(H_2O)(PO_3S_2C_{12}H_7)$ **(5)**; a= 22.1542(2) Å, b= 7.93590(10) Å, c= 15.1100(2) Å, β= 93.8460(10)°, V= 2650.56(5) $Å^3$ for $Co(H_2O)_2(PO_2OHS_2C_{12}H_7)_2$ **(6)**; a= 22.20022(9) Å, b= 8.01328(3) Å, c= 15. 22699(7) Å, β= 93.8226(4)°, V= 2702.80(2) $Å^3$ for $Mn(H_2O)_2(PO_2OHS_2C_{12}H_7)_2$ **(7)**.

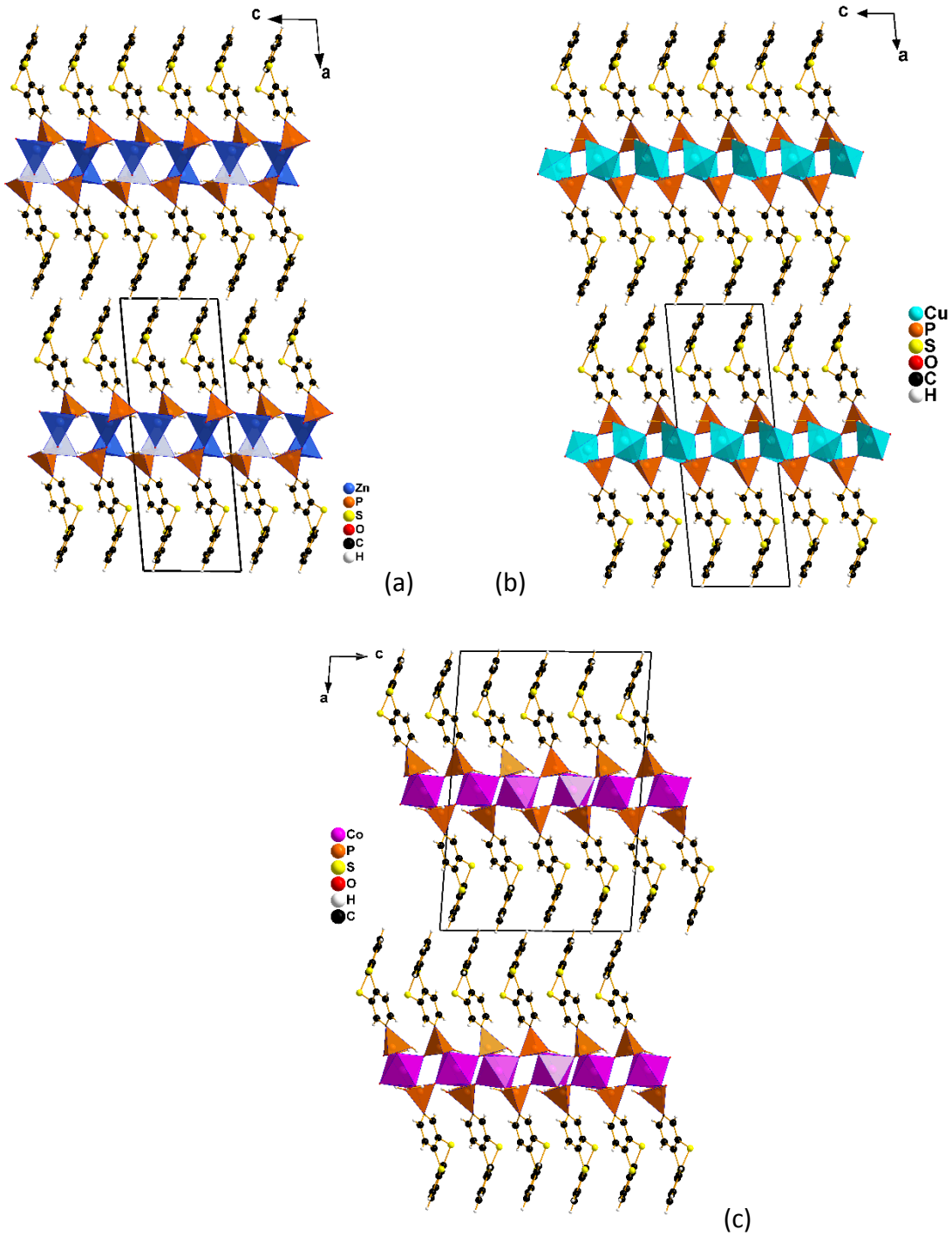

Figure 5: View of the lamellar structure of: (a) $Zn(H_2O)(PO_3S_2C_{12}H_7)$ **(4)**, (b) $Cu(H_2O)(PO_3S_2C_{12}H_7)$ **(5)** and (c) $Co(H_2O)_2(PO_2OHS_2C_{12}H_7)_2$ **(6)** projection along the *b* direction.

The structure of the inorganic framework of $Zn(H_2O)(PO_3S_2C_{12}H_7)$ **(4)** is composed of fully deprotonated PO_3C of the thianthrene phosphonic acid and distorted $ZnO_3(H_2O)$ tetrahedra sharing their corners to form infinite $[Zn(H_2O)PO_3C]_\infty$ inorganic layer regularly stacked along

the *a* direction **(Figure 6a)**. The Zn-O distances range from 1.903(2) Å to 1.983(2) Å and the P-O distances from 1.498(2) Å to 1.530(2) Å. The P-C distance is equal to 1.798(3) Å. Three apices of one $ZnO_3(H_2O)$ tetrahedron are sharing one oxygen with three PO_3C tetrahedra whereas the last apex is occupied by a water molecule in a free apical position distant from 1.983(2) Å. The molecules of water are located within the inorganic *bc* plane whereas the PO_3C tetrahedra, separated from each other by 7.8758(2) Å along the c direction and by 7.8428(2) Å along the *b* direction, are pointing outside the inorganic layer ensuring the connection with the $-C_{12}H_9S_2$ organic moiety.

Concerning the copper-based hybrid material of formula $Cu(H_2O)(PO_3S_2C_{12}H_7)$ **(5)** it presents an inorganic layer structure already encountered and described in the literature for the majority of the copper metallophosphonates of general formula $Cu(H_2O)PO_3R$ with a Cu/H_2O molar ratio equal to one **(Figure 6b)**.[48] Its inorganic framework is composed of isolated $Cu_2O_6(H_2O)_2$ copper(II) dimers connected by the fully deprotonated PO_3C tetrahedra of the phosphonic function. The Cu-O distances range from 1.925(3) Å to 2.384(3) Å, the P-O distances from 1.517(3) Å to 1.534(3) Å, and the P-C distance is equal to 1.800(4) Å. One dimer is composed of two $CuO_4(H_2O)$ distorted pyramids, sharing their apices with six oxygen of six phosphonate functions and two coordination-free water molecules. The two distorted pyramids share one edge through the two oxygen atoms located in an apical position with a $Cu\text{-}O_{apical}$ distance equal to 2.384(3) Å. Finally, the Cu-Cu distance is equal to 3.1836 (9) Å and the $Cu\text{-}O_{apical}\text{-}Cu$ angle is equal to 93.38(10)°.

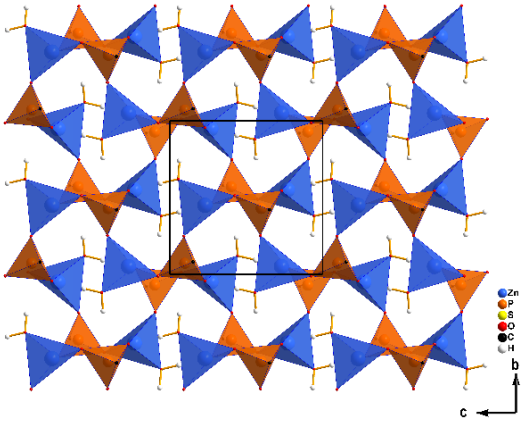

(a)

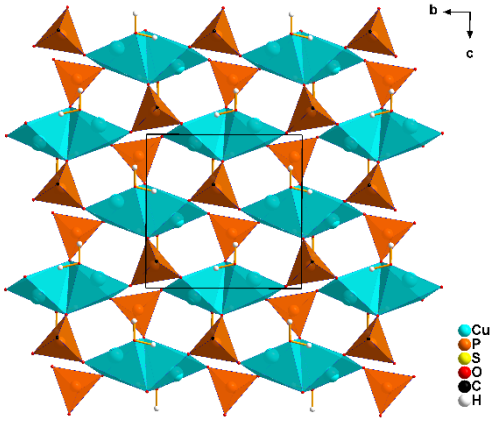

(b)

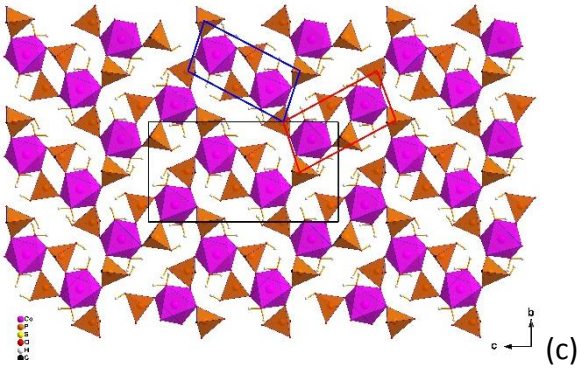

(c)

Figure 6: Representation of the inorganic layers of: (a) $Zn(H_2O)(PO_3S_2C_{12}H_7)$ **(4)**, (b) $Cu(H_2O)(PO_3S_2C_{12}H_7)$ **(5)** and (c) $Co(H_2O)_2(PO_2OHS_2C_{12}H_7)_2$ **(6)** projection along the *a* direction.

The $-C_{12}H_9S_2$ organic moieties of these copper and zinc-based materials are organized in a double layer stacked perpendicular to the *a* direction and are packed in columns along with the *b* directions **(Figure 7a-b)**. In one column all the C_6H_4 rings of the thianthrene moieties are pointing along the same direction, *b* or *-b*, and in the opposite direction in the adjacent column (depicted in red for the *b* direction and blue for the *-b* direction **(Figure SI 5)**. These two orientations and the bent geometry of the thianthrene phosphonic acid led to a peculiar 'Sawtooth' organization when the organic layer is observed along the *c* direction. The two organic sublayers are shifted by 1/2 along the *b*-axis, allowing their interweaving to form the double organic layer. The cohesion of the structure is ensured by C-H•••C and C-H•••S intracolumnar, intercolumnar, and interlayer interactions **(Figure SI 6 and SI 7; Table SI 2 and SI 3)**. The folding angles of the thianthrene moiety for this zinc **(4)** and copper-based material **(5)** were found equal to 130.5(2)° and 131.2(4)°, which are lower values than the one of 132.7(5)° found for the ligand.

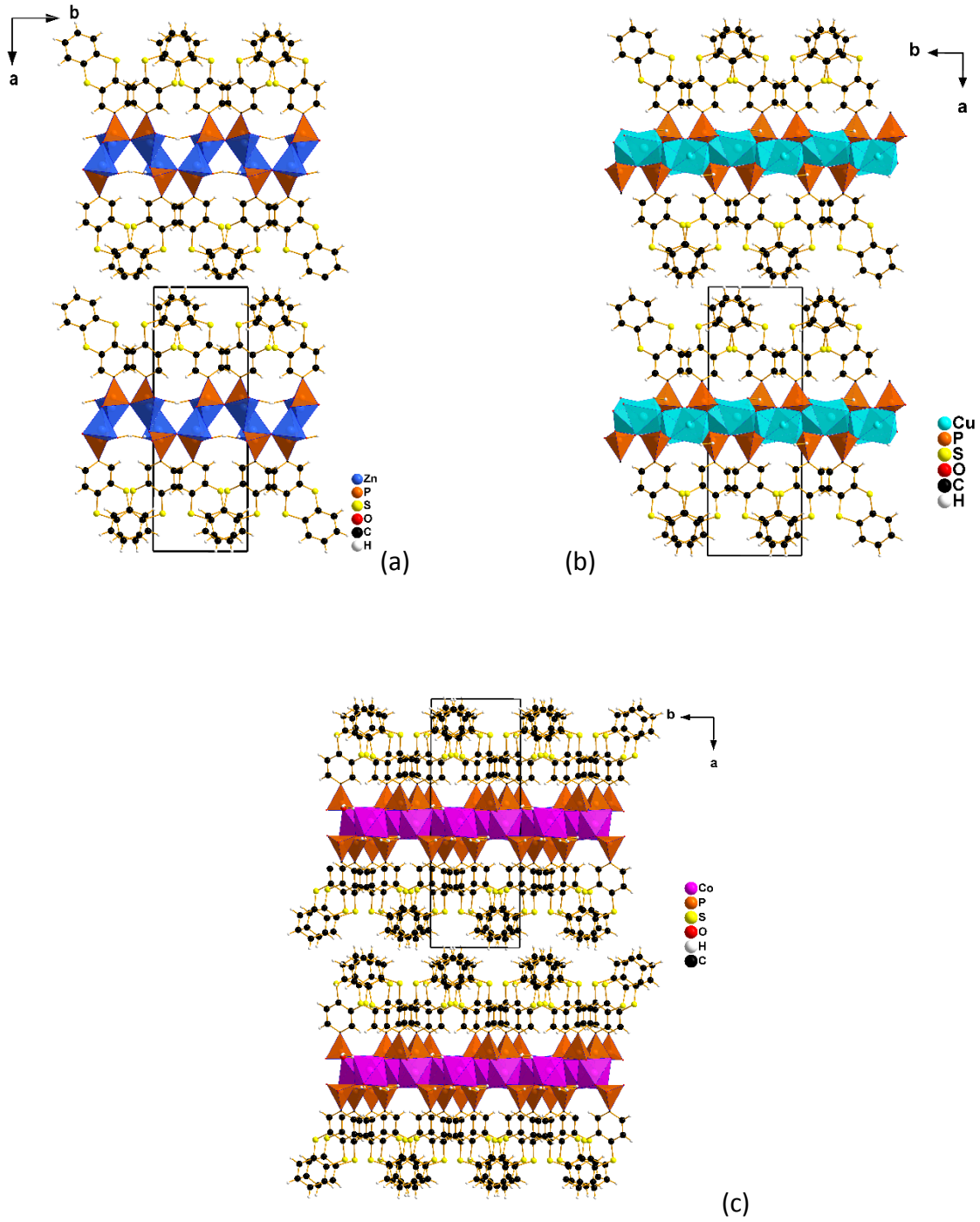

Figure 7: Representation of the layers structure of (a) $Zn(H_2O)(PO_3S_2C_{12}H_7)$ **(4)**, (b) $Cu(H_2O)(PO_3S_2C_{12}H_7)$ **(5)** and (c) $Co(H_2O)_2(PO_2OHS_2C_{12}H_7)_2$ **(6)** along the *c* direction.

At this stage, it is interesting to examine why these two compounds, which have a different inorganic sub-network, present a similar 'sawtooth' organization for their organic sub-network. The study of the arrangement of the polyhedra PO_3C, $ZnO_3(H_2O)$, and $CuO_4(H_2O)$ within the bidimensional *bc* cells of each compound has underlined several similarities. Thus, the two *bc* cells present remarkably close parameters of 7.8428(2) Å x 7.8758(2) Å (61.756

$Å^2$) for the zinc compound and 7.6616(2) Å x 7.5811(2) Å (58.078 $Å^2$) for the copper compound. In addition, the centers of the 2D cells as well as their apices are occupied by two PO_3C tetrahedra arranged in such a manner that their P-C bonds are respectively pointing outside the inorganic layer along with the *a* and -*a* direction. At last, the pattern formed by two $ZnO_3(H_2O)$ polyhedra located between the PO_3C tetrahedra present at the vertices of the 2D cell, is remarkably similar to that of the $CuO_4(H_2O)$ polyhedra forming one dimer with the main difference that these latter are not joined by an edge. All these similarities and probably the peculiar bend geometry of the thianthrene moiety may explain the common nature of the two organic sub-networks within these materials.

The cobalt and manganese compounds of formula $Co(H_2O)_2(PO_2OHS_2C_{12}H_7)_2$ **(6)** and $Mn(H_2O)_2(PO_2OHS_2C_{12}H_7)_2$ **(7)** present close cell parameters and isotype structures which differ from that of the copper **(4)** and zinc **(5)** based hybrid materials **(Figure 6c** and **Figure 7c,see Figure SI 5 for the structure of (7))**. Their inorganic sub-networks are composed of $MO_4(H_2O)_2$ polyhedra connected by the apices of the partially deprotonated (PO_2OHC) tetrahedra of the thianthrene phosphonic acid. Each $MO_4(H_2O)_2$ octahedra shares its apices with four oxygen of four phosphonate functions and two coordination-free water molecules. These polyhedra form an elementary brick $[M(H_2O)_2]_2[PO_2OH]_4$ (M=Co, Mn) located in the center of the *bc* cell **(Figure 6c)** in which two apices of one octahedron are bridged to another octahedron through four oxygen of two (PO_2OHC) tetrahedra while the other apices are occupied by four water molecules and four oxygen of the (PO_2OHC) tetrahedra pointing outside the brick. The M-O equatorial distances for the cobalt compound **(6)** and manganese compound **(7)** range from 2.035(5) Å to 2.121(5) Å and 2.1610(14) Å to 2.1869(14) Å respectively. The two $M\text{-}O_{water}$ apical distances of the octahedron are equal to 2.150(6) Å and 2.142(5) Å for **(6)** and for **(7)** equal to 2.217(2) Å and 2.2275(16) Å. The $O\text{-}M\text{-}O_{water}$ angles of the octahedra vary from 84.8(2)° to 94.9(2)° for **(6)** and 85.06(6)° to 97.18(8)° for **(7)**. Finally, the six P-O distances of each compounds present four short distances of 1.499(5) Å, 1.516(5) Å, 1.513(5) Å, 1.489(5) Å for **(6)**; 1.4885(15) Å, 1.5164(14) Å, 1.5020(14), 1.5161(14) for **(7)**) and two longest corresponding to the P-OH bonds equal to 1.584(5) Å and 1.582(5) Å for **(6)**; 1.5748(15) Å and 1.5750(14) Å for **(7)**. The organic subnetwork of these two compounds is constituted by the thianthrene moieties organized in a double layer shifted by 1/2 along the *b* direction. The $-C_{12}\ S_2H_7$ moieties are organized in a pair of columns

running along the *b* direction within which all the C_6H_4 rings are oriented along the same direction (*b* for example*)* and in the opposite direction in the two adjacent pairs (here -*b*). This arrangement leads to a 'sawtooth' pattern slightly different from the one observed for the copper or zinc materials, explained by a different organization and density of the (PO_2OHC) tetrahedra within the inorganic plane. As previously described in the case of copper and zinc-based hybrid materials, the inorganic layer is respectively composed either of tetrahedra or square-based pyramids connected to the corners of the PO_3C tetrahedra fully deprotonated. In the case of the cobalt and manganese-based compound, the inorganic layer is for its part composed of partially deprotonated (PO_2OHC) tetrahedra and $MO_4(H_2O)_2$ octahedra. The presence of one hydrogen atom on the PO_3C tetrahedra limits the number of connections with transition metal polyhedra and modifies the compactness of the inorganic network. In consequence, the bidimensional *bc* unit cell could be described as made up of two different patterns composed of two octahedra and four tetrahedra connected by the apices which only differ by their orientation as illustrated in **Figure 6c**. The presence of these two patterns leads to the doubling of the cell parameter along the c direction of ≈ 15 Å for **(6)** and **(7)** versus ≈ 7 Å for **(4)** and **(5)**.

As for the zinc and copper based materials, the cohesion of the structure of both compounds **(6)** and **(7)** is ensured by C-H•••C and C-H•••S intracolumnar, intercolumnar, and inter layer interactions **(Figure SI 8 and SI 9; and Table SI 4 and SI 5)**. The folding angle of the thianthrene moiety of the cobalt-based material **(6)** was found equal to 130.1(3)° and 130.1(2)° for the manganese-based material **(7)** and are both lower than the value of 132.7(5)° found for the ligand.

In light of the structural results obtained for all compounds, it appears that the structure of the hybrid compounds has very few impacts on the value of the folding angle of the thianthrene moiety located in the double organic layer as confirmed by the small differences observed: the value of 132.7(5)° found for the thianthrene phosphonic acid **(3)** is a slightly higher than the values of 130.5(2)° **(4)**, 131.2(4)° **(5)**, 130.1(3)° **(6)** and 130.1(2)° **(7)**.

Magnetic properties

The magnetic properties of $Cu(H_2O)(PO_3S_2C_{12}H_7)$ **(5)**, $Co(H_2O)_2(PO_2OHS_2C_{12}H_7)_2$ **(6)**, and $Mn(H_2O)_2(PO_2OHS_2C_{12}H_7)_2$ **(7)** have been studied as a function of temperature under a 1000 Oe magnetic field and are presented **Figure 8** and **9**. The fits of the $1/\chi = f(T)$ curves in the high-temperature region (above 150 K) (not shown) lead to Curie constants of 0.41, 2.74, and 4.21 emu·K·mol^{-1} for **(5)**, **(6)** and **(7)** respectively, in accordance with the expected values for Cu(II) ion (S = ½, C = 0.41 emu·K·mol^{-1} considering g = 2.1), high-spin Co(II) in an octahedral environment and high-spin Mn(II) in an octahedral environment[49] (S = 5/2, C = 4.375 emu·K·mol^{-1} considering g = 2.0) and negative Weiss temperatures of -8.0, -10 and -1 K, which indicate dominant antiferromagnetic interactions.

In accordance with its structure and previously published results on similar compounds [24, 25, 48, 50] the magnetic behavior of $Cu(H_2O)(PO_3S_2C_{12}H_7)$ **(5)** can be described considering isolated $Cu_2O_6(H_2O)_2$ copper(II) dimers **(Figure 8)**.

The data (χ and χT simultaneously) are fitted by Bleaney-Bowers' law[51] by using the spin Hamiltonian $\boldsymbol{H} = -J\boldsymbol{S}_{Cu1}\boldsymbol{S}_{Cu2} + g\beta H\boldsymbol{S}$ in which all parameters have their usual meaning, and the spin operator $\boldsymbol{S}$ is defined as $\boldsymbol{S} = \boldsymbol{S}_{Cu1} + \boldsymbol{S}_{Cu2}$. The fit leads to the following values: J = -4.45(5) cm^{-1} and g = 2.07(1).

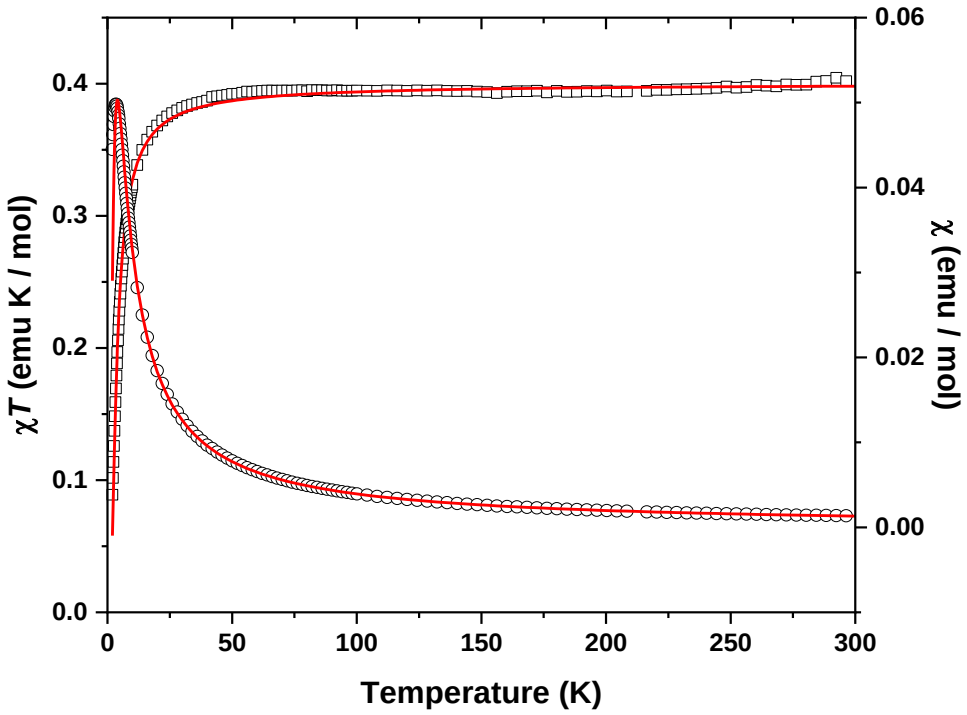

Figure 8: χ (black circles) and χT (black squares) as a function of temperature for $Cu(H_2O)(PO_3S_2C_{12}H_7)$ **(5)** under a magnetic field of 1000 Oe. Full red lines correspond to the best fit of the data (see text).

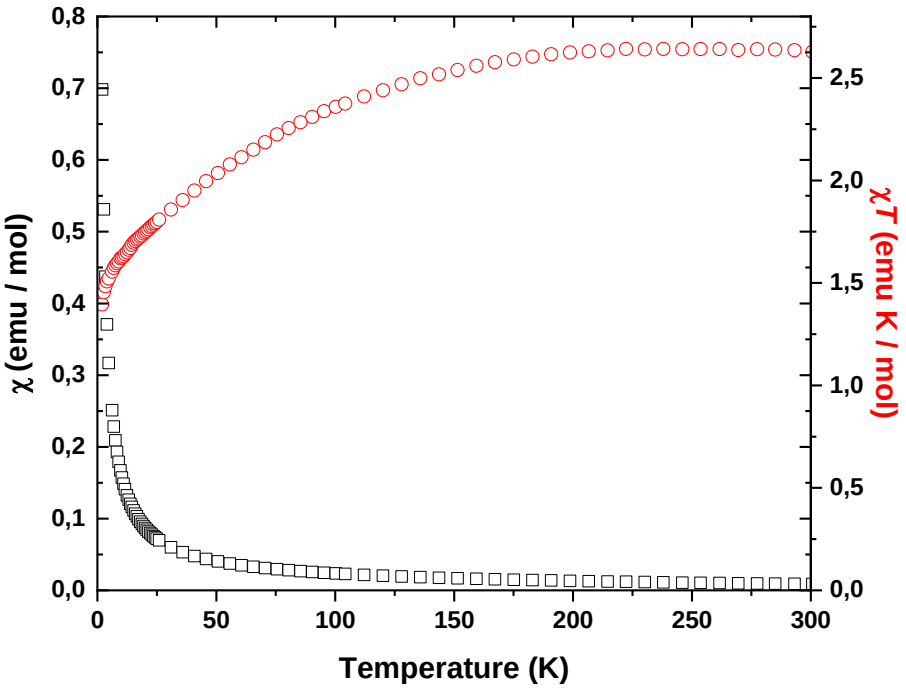

a)

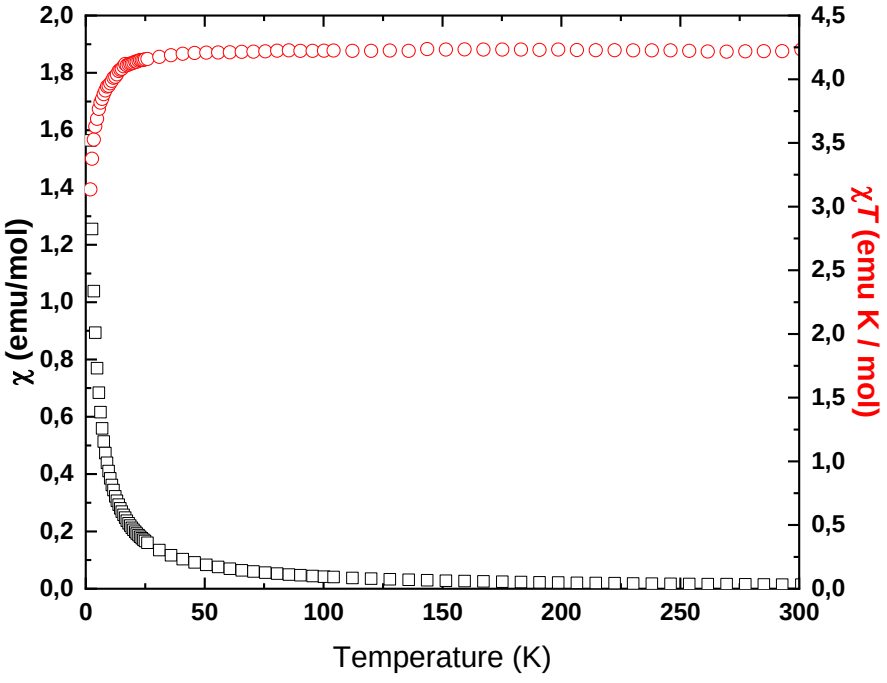

b)

Figure 9: χ (black square) and χT (red circle) as a function of temperature for compound a) $Co(H_2O)_2(PO_2OHS_2C_{12}H_7)_2$ **(6)** and b) $Mn(H_2O)_2(PO_2OHS_2C_{12}H_7)_2$ **(7)** under a magnetic field of 1000 Oe.

Magnetic properties from first-principles simulations

To confirm the magnetic properties identified experimentally, we have performed DFT simulations on $Cu(H_2O)(PO_3S_2C_{12}H_7)$ **(5)** , $Co(H_2O)_2(PO_2OHS_2C_{12}H_7)_2$ **(6)** and $Mn(H_2O)_2(PO_2OHS_2C_{12}H_7)_2$ **(7)** for two different magnetic orders: a ferromagnetic arrangement between all transition metal ions or an antiferromagnetic arrangement between nearest neighbor magnetic cations. Total energy differences between the two magnetic orders as well as the extracted magnetic moments for the three compounds and two DFT exchange-correlation functionals are reported in **Table 2**.

	PBEsol		**SCAN**	
	ΔE (K)	**μ (μ_B)**	**ΔE (K)**	**μ (μ_B)**
Cu (5)	17.46	0.73	6.14	0.73
Co (6)	103.55	2.72	38.47	2.75
Mn (7)	5.14	4.51	1.27	4.60

Table 2: Total energy differences and extracted magnetic moments for the three compounds obtained by the two exchange-correlation functionals PBEsol and SCAN.

Whatever the DFT functional, all three compounds are predicted to be antiferromagnetic materials. The computed magnetic moments on TM cations for the lowest energy state is compatible with a Cu^{2+} ($3d^9$, μ_{Cu}=1 μ_B), Mn^{2+} high spin state ($3d^5$, μ_{Mn}=5 μ_B) and Co^{2+} high spin state ($3d^7$, μ_{Co}=3 μ_B). Although these magnetic moments are constant with the functional, the energy difference between the ferromagnetic (FM) and antiferromagnetic (AFM) state is smaller for the three compounds using the more evolved SCAN functional. This may come from self-interaction errors that are better amended by this functional with respect to the PBEsol functional, notably for transition metal elements[52]. Nevertheless, the global trend in FM *vs.* AFM energies remains the same for the two functionals: the Cu based material is characterized by weak AFM interactions while the Co based compound has the largest AFM interactions. This is in sharp agreement with the Curie-Weiss temperatures found experimentally for the three compounds. By mapping our total

energy differences on a Heisenberg model of the form $H_{heisenberg} = -\sum_{i<j} J_{ij} S_i S_j$ where J_{ij} is the magnetic coupling between spins S at site i and j, we extract an average AFM coupling of -0.05 K, -4.1 K and -11.4 K for compounds based on Mn, Cu and Co respectively with the SCAN functional.

Luminescence properties

Absorbance

The UV/Vis absorbance spectra and the peaks obtained by fitting with a gaussian function for thianthrene phosphonic acid $PO(OH)_2S_2C_{12}H_7$ **(3)** and four different hybrid compounds $Zn(H_2O)(PO_3S_2C_{12}H_7)$ **(4)**, $Cu(H_2O)(PO_3S_2C_{12}H_7)$ **(5)**, $Co(H_2O)_2(PO_2OHS_2C_{12}H_7)_2$ **(6)**, and $Mn(H_2O)_2(PO_2OHS_2C_{12}H_7)_2$ **(7)**] are shown in **Figure 10a**. The fitting parameters are summarized in **Table SI 6**. Both thianthrene phosphonic acid and the four hybrid compounds exhibit absorption peaks - in the UV region near the visible range edge, with the Ligand, Co and Cu hybrids display a supplementary single absorption peak in the visible region.

Thianthrene phosphonic acid **(3)** and compounds exhibit multiple peaks, some common among all compounds and others specific to each. Thianthrene phosphonic acid **(3)** shows an intense peak at 4.58 eV (270 nm), followed by moderately intense peaks at 3.71 eV (333 nm), 3.40 eV (364 nm), and a broad weak peak at 2.44 eV (506 nm). Compound **(4)**, $Zn(H_2O)(PO_3S_2C_{12}H_7)$ displays an intense peak at 4.66 eV (265 nm), a moderately intense peak at 3.76 eV (329 nm), and a broad, low-intensity peak at 2.89 eV (429 nm). Compound **(5)**, $Cu(H_2O)(PO_3S_2C_{12}H_7)$ shows an intense peak at 4.72 eV (262 nm), followed by two moderately intense peaks at 3.71 eV (334 nm) and 3.08 eV (403 nm). Additionally, it shows a supplementary absorption peak at 1.66 eV (742 nm), attributed to the $^2E_g \rightarrow {}^2B_{1g}$ Cu^{2+} transition in tetrahedral coordination [53,54]. Compound **(6)**, $Co(H_2O)_2(PO_2OH\text{-}S_2C_{12}H_7)_2$ has an intense peak at 4.73 eV (262 nm), followed by one moderately intense peak at 3.72 eV (333 nm) and a low peak at 3.44 eV (360 nm), 2.75 eV (450 nm). Moreover, it exhibits an absorbance peak at 2.35 eV (528 nm), assigned to the Co^{2+} transition ^4T1_g (F) $\rightarrow$ $^4A_{2g}$ (F) or $^4T_{1g}$ (F) $\rightarrow$ $^4T_{1g}$ (P) [55,56,57]. Finally, compound **(7)**, $Mn(H_2O)_2(PO_2OH\text{-}S_2C_{12}H_7)_2$, displays an intense peak at 4.61 eV (269 nm), followed by one moderately intense peak at 3.81 eV (325 nm), a low-intensity peak at 3.52 eV (352 nm), and a broad weak peak at 2.97 eV (418 nm). Peaks located between 4.13 eV-3.44 eV (300-360 nm), and at 2.97 eV (418 nm) can be

partially assigned to the Mn^{2+} transition $^6A_{1g}(S) \rightarrow {}^4T_{2g}, {}^4E_g(D)$, and to $^6A_{1g}(S) \rightarrow {}^4T_{2g}, {}^4T_{1g}(G)$ or $^6A_{1g}(S) \rightarrow {}^4A_{1g}, {}^4E_g(G)$, [58] respectively.

The first peak **(AI)**, observed in the 4.73- 4.60 eV (262-269 nm) range, is intense in all the mentioned compounds, including the ligand (3), and is red-shifted compared to the absorption peaks of pure thianthrene at around 4.81 eV (258 nm), which is indicative of π-π* transition.[34] Previous studies [34,35] have shown that the peak position of thianthrene **(AI)** can be influenced by factors such as steric hindrance, conjugation[34]. Furthermore, thianthrene derivatives shows absorbance peaks were found ranging from 4.81-3.54 eV (258-350 nm) [34,35] in solid state and from 5.90-3.64 eV (210-340 nm) [59,60] in solution.

The second absorbance peak **(AII)** ranging from 3.80-3.71 eV (326-334 nm) is observed in both thianthrene phosphonic acid and the four compounds. This peak corresponds to a forbidden n- π* transition involving the non-bonding electrons of sulfur as reported by [30,34,35]. The third absorbance peak **(AIII)**, located in the 3.52- 3.40 eV (352-364 nm) range, is observed only for thianthrene phosphonic acid **(3)**, $Co(H_2O)_2(PO_2OH\text{-}S_2C_{12}H_7)_2$ **(6)**, and $Mn(H_2O)_2(PO_2OH\text{-}S_2C_{12}H_7)_2$ **(7)** compounds. This peak may be similar to the shoulders observed by P. Pander et al [34,35] and can be associated with the n- π* transition, similar to the second peak (II). The fourth peak **(AIV)** appearing at wavelengths of 2.45 eV (506 nm), 2.89 eV (429 nm), 3.08 eV (403nm), 2.75 eV (450 nm) and 2.97 eV (418 nm), respectively. Despite the blue shift observed in the peak **(AIV)** for compounds **(4)**, **(5)**, **(6)**, **(7)** compared to **(3)**, we assume a common origin of this peak. However, to our knowledge, these peaks are significantly red-shifted compared to the peaks reported for pure thianthrene and its derivatives, and therefore, their specific identification remains unknown. The fifth peak **(AV)** is identified in $Cu(H_2O)(PO_3S_2C_{12}H_7)$ **(5)** and $Co(H_2O)_2(PO_2OH\text{-}S_2C_{12}H_7)_2$ **(6)** compounds and is attributed to Cu^{2+} and Co^{2+} transitions, respectively. Therefore, the ligand **(3)** and compounds **(4, 5, 6, 7)** exhibit three identical peaks **(AI)**, **(AII),** and **(AIII)** corresponding to π-π* and n-π* transitions, which are the characteristic features of the thianthrene absorption spectrum. These four peaks, being the most intense, indicate that the main mechanism of optical absorption is governed by the common thianthrene moiety present in both the ligand and the compounds. Additionally, specific additional peaks **(AIV)** and **(AV)** are observed in compounds **(5)** and **(6)** due to the specific transitions attributed to Co^{2+} and Cu^{2+} transitions, respectively.

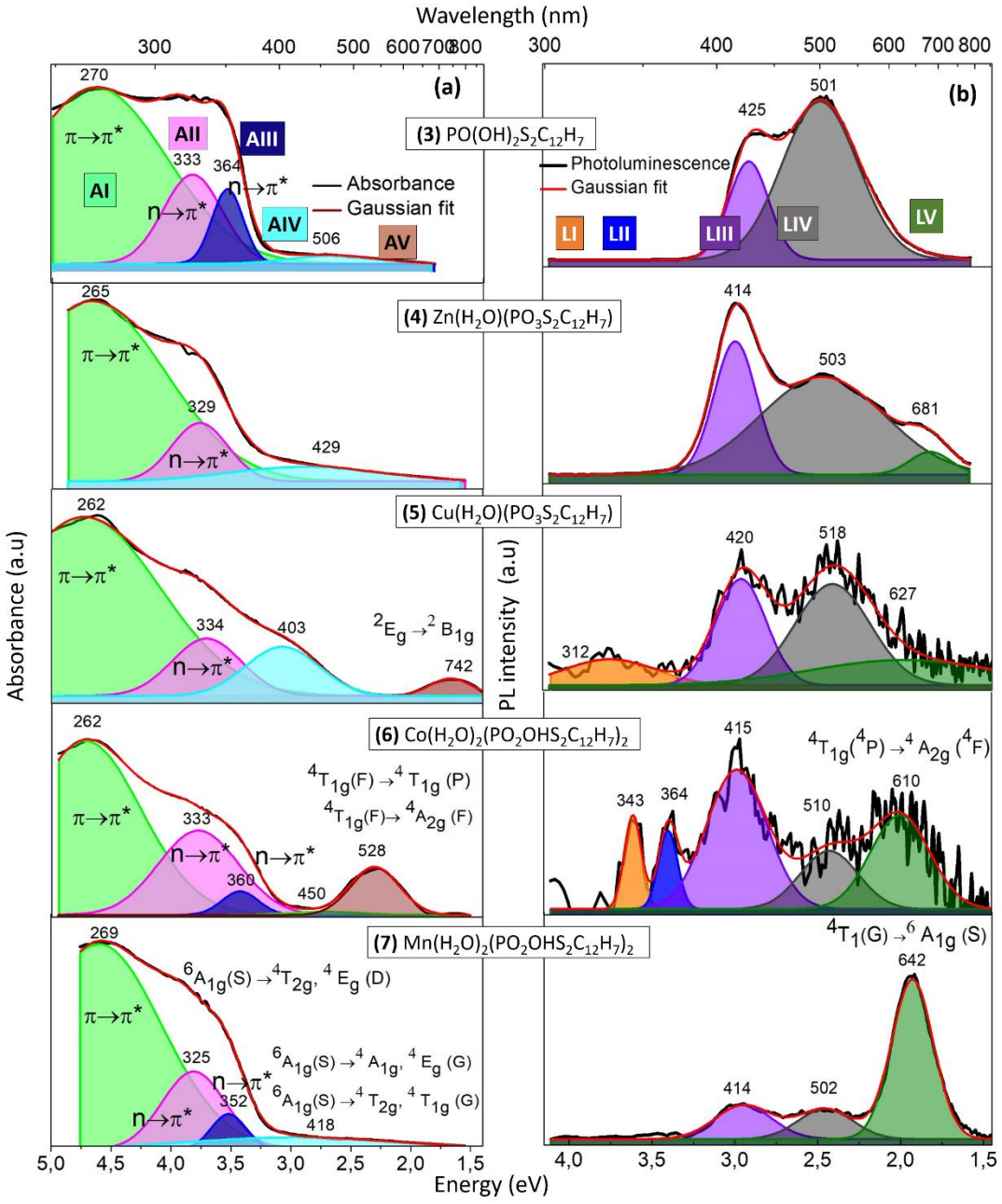

Figure 10: Absorbance (a) and Photoluminescence with excitation at 4.66eV (266 nm) (b) spectra of thianthrene phosphonic acid $PO(OH)_2S_2C_{12}H_7$ **(3)** and hybrid compounds, $Zn(H_2O)(PO_3S_2C_{12}H_7)$ **(4)**, $Cu(H_2O)(PO_3S_2C_{12}H_7)$ **(5)**, $Co(H_2O)_2(PO_2OH\text{-}S_2C_{12}H_7)_2$ **(6)** and $Mn(H_2O)_2(PO_2OH\text{-}S_2C_{12}H_7)_2$ **(7)**] absorbance and emission peaks fitted by Gaussian functions.

Photoluminescence

Similarly as absorbance, the Photoluminescence (PL) spectra of thianthrene phosphonic acid **(3)** and four different hybrid compounds **(4)**, **(5)**, **(6)** and **(7)** are displayed in **Figure 10b**. The emission spectra were fitted using Gaussian functions, and the fitted parameters are summarized in **Table SI 6**. Thianthrene phosphonic acid **(3)** exhibits two strong emission peaks at 2.92 eV (425 nm) **(LIII)** and 2.47 eV (501 nm) **(LIV)**. Previous studies on thianthrene derivatives have reported similar fluorescence and phosphorescence emissions within the same wavelength range for the crystalline form, solution at room temperature, and under vacuum conditions.[61,62] The compound $Zn(H_2O)(PO_3S_2C_{12}H_7)$ **(4)** displays three emission peaks: a strong peak at 2.99 eV (414 nm) **(LIII)**, a moderately intense peak at 2.46 eV (503 nm) **(LIV)**, and a weak peak at 1.82 eV (681 nm) **(LV)**. Interestingly, the two peaks **(LIII)** and **(LIV)** are nearly at the same wavelength (energy) as the ones of thianthrene phosphonic acid **(3)**. The spectral similarity between the ligand and hybrid compounds provides evidence of a common origin for these two peaks. The **(LV)** peak at 1.82 eV (681 nm) in the Zn **(4)** compound cannot be attributed to the presence of Zn^{2+} ions due to their full $3d^{10}$ electronic configuration, which prevents electron promotion to higher energy levels within the visible range. The $Cu(H_2O)(PO_3S_2C_{12}H_7)$ **(5)** compound exhibits three emission peaks at 3.97 eV (312 nm) **(LI)**, 2.95 eV (420 nm) **(LIII)** , and 2.39 eV (518 nm) **(LIV)**, 1.97 eV (627 nm) **(LV)** which are characterized by a weak peak **(LI)**, followed by two equally intense **(LIII), (LIV),** and **(LV)**. Despite the Cu^{2+} element being known as an emission quencher in studies,[63,64] the two most intense peaks can be attributed to the same transition observed in the ligand **(3)**. The $Co(H_2O)_2(PO_2OH\text{-}S_2C_{12}H_7)_2$ **(6)** compound presents several emission peaks at 3.61 eV (343 nm) **(LI)**, 3.40 eV (364 nm) **(LII)**, 2.98 eV (415 nm) **(LIII)**, 2.43 eV (510 nm) **(LIV)** and, 2.0 eV (610 nm) **(LV)**. Similar to compound **(5),** the Co **(6)** compound exhibits low-intensity emission peaks compared to the other compounds, just slightly above the background level. The Co **(6)** compound shows two weak peaks at 3.61 eV (343 nm) **(LI)**, and 3.40 eV (364 nm) **(LII)** that remain unidentified. The most intense peak **(LIII)** and moderate intense peak **(LIV)** can be assigned to the same transition observed in the ligand **(3)**, while the broad peak **(LV)** is blue-shifted compared to **(4)** and **(5)** and may be attributed to the transition of Co^{2+} in octahedral coordination $^4T_{1g}(F) \rightarrow {}^2T_{1g}$[65]). The $Mn(H_2O)_2(PO_2OH\text{-}S_2C_{12}H_7)_2$ **(7)** compound

displays three-emission peaks at 2.98 eV (414 nm) **(LIII)**, 2.46 eV (502 nm) **(LIV)** and 1.93 eV (642 nm) **(LV)**. The spectral similarity between the ligand and hybrid compounds suggests a shared origin for these two peaks. The **(LV)** peak at 1.93 eV (642 nm) in the Mn **(7)** hybrid compound can be assigned to the spin forbidden $^4T_{1g}(G) \rightarrow {}^6A_{1g}$ transition of Mn^{2+} [58,66,67]. The LV band, observed in compounds (**4**), (**5**), (**6**), and (**7**), displayed variations in peak position and intensity. In (**4**) and (**5**), the LV peak's origin was not linked to Zn^{2+} or Cu^{2+}, respectively. However, in (**6**) and (**7**), their positions could be correlated with Co^{2+} and Mn^{2+} ions transitions. While a shared origin, possibly from a common organic moiety, is plausible for the LV band in all four compounds, reported transitions in (**6**) and (**7**) may also contribute. Thus, the exact origin of the LV band remains uncertain.

PL decay time measurements were conducted on samples at different detection wavelengths, following the previously described conditions. The decay time of all the compounds were fitted using different models (single, double exponential, mean decay time…). Ultimately, the mean decay model[68]was deemed the most relevant, and the corresponding values are presented in **Table** 3. Specifically, for the peaks where photoluminescence (PL) decay times can be detected, they are provided in **Table 4**. Upon observing the general decay times pattern, it becomes evident that all the compounds exhibit similar behavior in decay times. For instance, the mean decay time of Thianthrene phosphonic acid $PO(OH)_2S_2C_{12}H_7$ **(3)** was measured at emission peaks of 2.92 eV (425 nm) **(LIII)** and 2.47 eV (501nm) **(LIV)**, resulting in decay times of 5 µs and 6 µs, respectively (displayed in **Figure SI 7)**. This small decay time difference at those two peaks (**LIII)** and (**LIV)**, as reported in **Table** 3**,** is consistent across all the other compounds, except for the Cu compound where the difference is reversed. Earlier studies[31] reported that pure thianthrene compounds exhibit fluorescence with decay time in the nanoseconds range at 2.92 eV (425 nm), while room temperature phosphorescence (RTP) occurs with decay time in the milliseconds range at 2.47 eV (501 nm). In the higher energy region, at 3.97 eV (312 nm) for compound **(5)**, no detectable emission decay curve was observed. For compound **(6)** at 3.62 eV (342 nm) and 3.40 eV (364 nm), the decay times were measured to be 5.71 µs and 6.60 µs, respectively. At longer wavelengths, specifically for peak **(LV)**, the average decay

times were found to be within a comparable range of 17.47 µs for compound **(4)**, 20.8 µs for compound **(6)**, 10.85 µs for compound **(7)**.

According to literature,[31] the thianthrene derivative shows the coexistence of fluorescence and phosphorescence at room temperature (RT). The emission peaks observed in the thianthrene derivative arise from the lowest singlet state (S1), spin-forbidden lowest triplet state (T_1), and potentially from spin-forbidden upper triplet manifold (T_n) excited states, involving transitions of π-π* and n-π* character or mixed of both. The emission peaks (**LIII)** and (**LIV)**, as mentioned previously, possess the spectral characteristics associated with recombination from the upper singlet and triplet states, respectively. However, the room temperature lifetimes show minimal differences between these two transitions or with other observed transitions. Hence, it is challenging to conclusively demonstrate the triplet nature of peak **(LIV)** or any other excited level observed by photoluminescence.[33]

In our case, a strong spin-orbit coupling (SOC) potentially induced by the folding of the thianthrene molecule could be present, given the variation in folding angle from 132° to 130°. However, SOC modifications were not observed due to the limited range of folding angle variation studied. The reason behind the comparable radiative recombination lifetimes found for peaks (**LIII)** and (**LIV)**, assumed to arise from singlet and triplet states, are not yet fully understood. The presence of strong SOC could have an influence on the processes of intersystem crossing (ISC) and reverse intersystem crossing (RISC), which could potentially lead to significant modifications in the observed recombination decay time[31]. Additionally, some authors[58,69] have reported the sensitivity of thianthrene derivatives triplet state to oxygen. Considering that the measurements were conducted in ambient air, the presence of oxygen may be a factor influencing the measured recombination time of peak (**LIV)**, which might correspond to a triplet state with modified decay time.

Compounds	**Peak Decay time (µs)**				
Peaks	**LI**	**LII**	**LIII**	**LIV**	**LV**
(3)			5.07	5.84	
(4)			4.27	4.97	17.47
(5)			8.32	7.36	

(6)	5.71	6.60	6.98	7.70	20.8
(7)			4.18	4.70	10.85

Table 3: Tabulated luminescence peaks and corresponding mean decay time for the thianthrene phosphonic acid and the *hybrid compounds* $PO(OH)_2S_2C_{12}H_7$ **(3),** $Zn(H_2O)(PO_3S_2C_{12}H_7)$ **(4)**, $Cu(H_2O)(PO_3S_2C_{12}H_7)$ **(5)**, $Co(H_2O)_2(PO_2OH\text{-}S_2C_{12}H_7)_2$ **(6)** and $Mn(H_2O)_2(PO_2OH\text{-}S_2C_{12}H_7)_2$ **(7)** and the excitation wavelength 266nm.

Conclusion

The original bent rigid molecule thianthrene-2-ylphosphonic acid was synthesized from 2-bromothianthrene, and was further used for the hydrothermal synthesis of four transition metallophosphonates $M(H_2O)PO_3\text{-}S_2C_{12}H_7$ (M = Cu, Zn) and $M(H_2O)_2(PO_2OH\text{-}S_2C_{12}H_7)_2$ (M = Mn, Co). The obtained materials were in the form of polycrystalline powders, their structures were determined using X-ray diffraction on single crystals. All four materials exhibit a lamellar structure, with variations in the nature and architecture of their inorganic layers. The zinc-based material featured an inorganic layer where PO_3C and $ZnO_3(H_2O)$ tetrahedra are sharing their corners. In contrast, the inorganic layer of the copper hybrid consisted of isolated $Cu_2O_6(H_2O)_2$ copper(II) dimers, which were connected by the PO_3C tetrahedra of the phosphonic function. The cobalt and manganese materials had an isotype inorganic layer composed of $MO_4(H_2O)_2$ octahedra (M=Co or Mn) connected by the apices to partially deprotonated (PO_2OHC) tetrahedra of thianthrene phosphonic acid. The organic network of these materials exhibits a double-layer organization, with the molecules arranged in a sawtooth pattern. The magnetic properties of the Cu, Co, and Mn compounds were investigated by studying the variation of susceptibility with temperature. The negative values of the Weiss temperatures indicate the presence of dominant antiferromagnetic interactions. The magnetic behavior of the copper dimers was fitted by using the Bleaney-Bowers' law, which allowed for the determination of the antiferromagnetic interaction energy between copper atoms (J = -4.45(5) cm^{-1}). These antiferromagnetic behaviors were further theoretically supported by Density Functional Theory, which confirmed an antiferromagnetic arrangement between nearest neighbor magnetic cations, as opposed to a ferromagnetic arrangement between all transition metal ions. Furthermore, the absorbance, and luminescence properties of thianthrene phosphonic acid $PO(OH)_2S_2C_{12}H_7$ **(3)** and four different hybrid compounds $Zn(H_2O)(PO_3S_2C_{12}H_7)$ **(4)**, (b) $Cu(H_2O)(PO_3S_2C_{12}H_7)$ **(5)**,

$Co(H_2O)_2(PO_2OH\text{-}S_2C_{12}H_7)_2$ **(6)** and $Mn(H_2O)_2(PO_2OH\text{-}S_2C_{12}H_7)_2$ **(7)**] were investigated. The results revealed multiple excitation and recombination mechanisms. The main contribution to absorption and emission in all compounds **(3)**, **(4)**, **(5)**, **(6)** and **(7)** was identified to originate from organic moiety. However, compounds **(5)**, **(6)** and **(7)** exhibited additional absorbance and emission peaks attributed partially or mainly to the presence of Cu, Co, and Mn transition metals, respectively. Recombination with transition character of π-π* and n-π* or a combination of both types was observed originating from the organic moiety of the compounds. Singlet and triplet state recombination may have also been observed; however, an unidentified quenching mechanism may be responsible for reducing the lifetime of the triplet state. In this study, the four crystalline hybrid materials (**4**-**7**) possess a 2D structure. We can postulate that the incorporation on TPA of a second function having the capacity to form iono-covalent bonds with a metallic salt (e.g. phosphonic acid, carboxylic acid) could help in the production 3D hybrid structure. A second strategy to produce 3D structures would consist of using metallic salts (e.g. silver[70]) or a mixture of metallic salts that could interact with both phosphonic acid function and the sulfur atoms of TPA in a coordination network.

Author statement:

Geoffrey Letheux: Formal Analysis; Resources; Investigation; Writing – review & editing. ***Olivier Perez:*** Formal Analysis, Investigation, Validation, Writing – review & editing. ***Parameshwari Ganesan:*** Formal Analysis; Data curation; Investigation; Writing – review & editing. ***Julien Cardin:*** Conceptualization; Formal Analysis; Funding acquisition; Data curation; Investigation; Writing – original draft; Writing – review & editing. ***Christophe Labbé:*** Formal Analysis; Investigation; Data curation, Writing – review & editing. ***Fabien Veillon:*** Formal Analysis ; Investigation. ***Guillaume Rogez:*** Formal Analysis; Data curation; Investigation; Writing – original draft; Writing – review & editing. ***Julien Varignon:*** Data curation; Formal Analysis, Methodology; Writing – original draft; Writing – review & editing. ***Mathilde Ligeour:*** Investigation; Resources. ***Paul-Alain Jaffrès:*** Conceptualization; Investigation; Resources, Writing – original draft; Writing – review & editing. ***Jean-Michel Rueff:*** Conceptualization; Funding acquisition; Resources; Investigation; Project administration; Supervision; Writing – original draft; Writing – review & editing.

There are no conflicts to declare.

Acknowledgements

The authors acknowledge the financial support of the French Agence Nationale de la Recherche LabEx EMC3 through the Project MAHYTER (Grant No. 10-LABX-0009), and the Normandy Region (Réseau d'Intérêt Normand - Label d'excellence)

The authors thank Professor Vincent Caignaert for helpful discussions, and the platforms (RMN-RPE and spectrométrie de masse) from the University of Brest.

References

[1] K. Biradha, A. Ramanan, J.J. Vittal, *Cryst. Growth Des*., **2009**, *9*, 2969–2970.

[2] J.M. Rueff, V. Caignaert, A. Leclaire, C. Simon, J.P. Haelters, P.A. Jaffrès, *CrystEngComm.*, **2009**, *11*, 556-559.

[3] L. Tang, S. Zhang, Q. Wu, X. Wang, H. Wu, Z. Jiang, *J. Mater. Chem. A*, **2018**, *6*, 2964-2973.

[4] B. Iqbal, M. Saleem, S. N. Arshad, J. Rashid, N. Hussain, M. Zaheer, *Chem. Eur. J*., **2019**, *25*, 10490-10498.

[5] Y. Rachuri, B. Parmar, K.K. Bisht, E. Suresh, *Dalton Trans.*, **2016**, *45*, 7881-7892.

[6] K. Otsubo, S. Nagayama, S. Kawaguchi, K. Sugimoto, H. Kitagawa, *JACS Au*, **2022**, *2*, 109−115.

[7] G. Rogez, N. Viart, M. Drillon, *Angew. Chem. Int. Ed*., **2010**, *49*, 1921-1923.

[8] Q. Evrard, Z. Chaker, M. Roger, C. M. Sevrain, E. Delahaye, M. Gallart, P. Gilliot, C. Leuvrey, J.-M. Rueff, P. Rabu,C. Massobrio, M. Boero, A. Pautrat, P.-A. Jaffrès, G. Ori, G. Rogez, *Adv. Funct. Mater*., **2017**, *27*, 1703576.

[9] T. Basu, C. Bloyet, F. Beaubras, V. Caignaert, O. Perez, J.-M. Rueff, A. Pautrat, B. Raveau, J.-F. Lohier, P.-A. Jaffrès, H. Couthon, G. Rogez, G. Taupier, H. Dorkenoo, *Adv. Funct. Mater.*, **2019**, *29*, 1901878.

[10] J.M. Rueff, O. Perez, V. Caignaert, G.B. Hix, M. Berchel, F. Quentel, P.A. Jaffrès, *Inorg. Chem.*, **2015**, *54*, 2152-2159.

[11] B. N. Yalamandala, W.T. Shen, S.H. Min, W.H. Chiang, S.J. Chang, S.H. Hu, *Adv. NanoBiomed Res*., **2021**, *1*, 2100014.

[12] V. Pascanu, G. González Miera, A. K. Inge, B. Martín-Matute, *J. Am. Chem. Soc*., **2019**, *141*, 7223-7234.

[13] A. E. Thorarinsdottir, T. D. Harris, *Chem. Rev*., **2020**, *120*, 8716-8789.

[14] L. Hamon, P. L. Llewellyn, T. Devic, A. Ghoufi, G. Clet, V. Guillerm, G. D. Pirngruber, G. Maurin, C. Serre, G. Driver, W. van Beek, E. Jolimaitre, A. Vimont, M. Daturi, G. Ferey, *J. Am. Chem. Soc*., **2009**, *131*, 17490-17499.

[15] M. Berchel, T. Le Gall, C. Denis, S. Le Hir, F. Quentel, C. Elléouet, T. Montier, J.M. Rueff, J.Y. Salaün, J.P. Haelters, P. Lehn, G.B. Hix, P.A. Jaffrès, *New J. Chem*., **2011**, *35*, 1000-1003.

[16] A. Ringaci, A.V. Yaremenko, K.G. Shevchenko, S.D. Zvereva, M.P. Nikitin, *Chem. Eng. J*., **2021**, *418*, 129386.

[17] S. Chand, O. Alahmed, W. S. Baslyman, A. Dey, S. Qutub, R. Saha, Y. Hijikata, M. Alaamery, N. M. Khashab, *JACS Au*, **2022**, *2*, 623-630.

[18] A. Schneemann, V. Bon, I. Schwedler, I. Senkovska, S. Kaskel, R. A. Fischer, *Chem. Soc. Rev*., **2014**, *43*, 6062-6096.

[19] V.M. Georgieva, E.L. Bruce, M.C. Verbraeken, A.R. Scott, W.J. Casteel Jr., S. Brandani, P.A. Wright, *J. Am. Chem. Soc*., **2019**, *141*, 12744-12759.

[20] C.T. Yang, A.R. Kshirsagar, A.C. Eddin, L.C. Lin, R. Poloni, *Chem. Eur. J.,* **2018**, *24*, 15167-15172.

[21] A. C. McKinlay, J. F. Eubank, S. Wuttke, B. Xiao, P. S. Wheatley, P. Bazin, J. C. Lavalley, M. Daturi, A. Vimont, G. De Weireld, P. Horcajada, C. Serre, R. E. Morris, *Chem. Mater*., **2013**, *25*, 1592.

[22] M. Bonneau, C. Lavenn, J.-J. Zheng, A. Legrand, T. Ogawa, K. Sugimoto, F.-X. Coudert, R. Reau, S. Sakaki, K.-i. Otake and S. Kitagawa, *Nature Chem*., **2022**, *14*, 816-822.

[23] J.M. Rueff; G.B. Hix, P.A. Jaffrès, Book chapter in "Tailored Organic–Inorganic Materials", First Edition, chapter 9, p341-393. 2015 John Wiley & Sons, Inc. Published **2015** by John Wiley & Sons, Inc.

[24] J.M. Rueff, V. Caignaert, S. Chausson, A. Leclaire, C. Simon, O. Perez, L. le Pluart, P.A. Jaffrès, *Eur. J. Inorg. Chem*., **2008**, 4117-4125.

[25] N. Hugot, M. Roger, J.M. Rueff, J. Cardin, O. Perez, V. Caignaert, B. Raveau, G. Rogez, P.A. Jaffrès, *Eur. J. Inorg. Chem*., **2016**, 266-271.

[26] O. Perez, C. Bloyet, J.M. Rueff, N. Barrier, V. Caignaert, P.A. Jaffrès, B. Raveau, *Crystal Growth Des*., **2016**, *16*, 6781–6789.

[27] J.M. Rueff, O. Perez, A. Pautrat, N. Barrier, G. Hix, S. Hernot, H. Couthon-Gourvès, P.A. Jaffrès, *Inorg. Chem*., **2012**, *51*, 10251-10261.

[28] P. Pander, A. Swist, R. Turczyn, S. Pouget, D. Djurado, A. Lazauskas, R. Pashazadeh, J. V. Grazulevicius, R. Motyka, A. Klimash, P. J. Skabara, P. Data, J. Soloducho, F. B. Dias, *J. Phys. Chem. C.*, **2018**, *122*, 24958-24966.

[29] J. G. Liu, Y. Nakamura, Y. Shibasaki, S. Ando, M. Ueda, *Macromolecules*, **2007**, *40*, 4614-4620.

[30] A. Tomkeviciene, A. Dabulienė, T. Matulaitis, M. Guzauskas, V. Andruleviciene, J. V. Grazulevicius, Y. Yamanaka, Y. Yano, *Dyes Pigm.* **2019,** *170*, 107605.

[31] H. Liu, Y. Gao, J. Cao, T. Li, Y. Wen, Y. Ge, L. Zhang, G. Pan, T. Zhou, B. Yang, *Mater. Chem. Front.*, **2018,** *2*, 1853-1858.

[32] J. Mei, Y. Hong, J. W. Y. Lam, A. Qin, Y. Tang, B. Z. Tang, *Adv. Mater.*, **2014**, *26*, 5429–5479.

[33] K. Sun, W. Jiang, X. Ban, B. Huang, Z. Zhang, M. Ye, Y. Sun, *RSC advances,* **2016**, *6*, 22137-22143.

[34] P. Pander, A. Swist, J. Soloducho, F. B. Dias, *Dyes Pigm.,* **2017**, *142*, 315-322.

[35] P. Pander, A. Swist, R. Turczyn, S. Pouget, D. Djurado, A. Lazauskas, F. B. Dias, *J. Phys. Chem. C.*, **2018**, *122*, 24958-24966.

[36] D. Deubel, *J. Org. Chem*., **2001**, *66*, 2686-2691.

[37] O. Dolomanov, L. Bourhis, R. Gildea, J.Howard, H.Puschmann. *J. Appl. Crystallogr.*, **2009**, *42*, 339-341.

[38] G. Kresse, J. Furthmüller, *Comput. Mater. Sci.,* **1996***, 6*, 15-50.

[39] G. Kresse, J. Hafner, *Phys. Rev. B,* **1993**, *47*, 558(R).

[40] P. E. Blöchl, *Phys. Rev. B,* **1994***, 50*, 17953.

[41] J. P. Perdew, A. Ruzsinszky, G. I. Csonka, O. A. Vydrov, G. E. Scuseria, L. A. Constantin, X. Zhou, K. Burke *Phys. Rev. Lett.*,**2009**, *100*, 136406.

[42] J. Sun, A. Ruzsinszky, J. P. Perdew, *Phys. Rev. Lett.*, **2015**, *115*, 036402.

[43] C. Burkhart, G. Haberhauer, *Eur. J. Org. Chem*., **2017**, 1308-1317.

[44] G. Xie, X. Li, D. Chen, Z. Wang, X. Cai, D. Chen, Y. Li, K. Liu, Y. Cao, S.J. Su, *Adv. Mater*., **2016**, *28*, 181-187.

[45] A. Le Bail. Powder Diffraction, **2005**, *20*, 316.

[46] A. Chandra, T. Zeegers-Huyskens. *J. Phys. Chem.*, *A*, **2005**, *109*, 12006-12013.

[47] S. Larson, S. Simonsen, G. Martin, K. Smith, S. Puig-Torres. *Acta Cryst C.*, **1984**, *40*, 103-106.

[48] C. Bloyet, M. Rogez, J.-M. Rueff, B. Raveau, J.-F. Lohier, G. Rogez, P.-A. Jaffrès. *Eur. J. Inorg. Chem*., **2016**, 28, 4643–4648.

[49] R. L. Carlin, Magnetochemistry, Springer-Verlag, Berlin, **1986**.

[50] J. Le Bideau, C. Payen, P. Palvadeau, B. Bujoli, *Inorg. Chem*., **1994**, *33*, 4885-90.

[51] B. Bleaney, K. D. Bowers. Proc. Roy. Soc. (London) Ser. A 214 (**1952**): 451

[52] J. Varignon, M. Bibes, A. Zunger, *Phys. Rev. B.*, **2019**, *100*, 035119.

[53] S. D. Dević, Z. V. Popović, A. Breitschwerdt, G. Dhalenne, A. Revcolevschi, P*hys. Status Solidi B*, **1997,** *203*, 579-584.

[54] B. S. Bae, M. C. Weinberg . *J. Non-Cryst. Solids,* **1994**, *168*, 223-231.

[55] G. Cheng, H. Hu. J. Xia,Y. Zhu, B. Chen, *Mater. Res. Express,* **2018**, *5*, 066201.

[56] W. Künzel, W. Knierim, U. Dürr, *Opt. Commun*. **1981**, *36*, 383-386.

[57] M. Duarte, E. Martins, S. L. Baldochi, S. P. Morato, Jr. N. D. Vieira, M.M. Vieira, *Opt. commun.* **1998,** *151*,366-373.

[58] M. Kawano,H. Takebe, M. Kuwabara, *Opt. Mater.* **2009**, *32*, 277-280.

[59] M. Samoć, A. Samoć, D. F. Williams, *J. Chem. Phys.,* **1982,** *76*, 3768-3773.

[60] K. Leitonas, A. Tomkeviciene, G. Baratte, A. Dabuliene, S. M. Punniyakoti, D. Volyniuk, J. V. Grazulevicius, *Sens. Actuators B: Chem.,* **2021**, *345*, 130369.

[61] A. Arena, S. Campagna, A. M. Mezzasalma, R. Saija, G. Saitta, *Il Nuovo Cimento D.*, **1993**, *15*, 1521-1532.

[62] Y. Wen, H. Liu, S. T. Zhang, G. Pan, Z. Yang, T. Lu, B. Li, J. Cao, B. Yang, *CCS Chem.,* **2021**, *3*, 1940-1948.

[63] F. Beaubras, J. M. Rueff, O. Perez,F. Veillon, V. Caignaert, J. F. Lohier, P. A. Jaffres, *Dalton Trans.,* **2020**, *49*, 3877-3891.

[64] Z. C. Liu, Z. Y. Yang, T. R. Li, B. D. Wang, Y. Li, D. D. Qin, M. H. Yan, *Dalton Trans.*, **2011**, *40*, 9370-9373.

[65] G. Nagarjuna, T. Satyanarayana, Y. Gandhi, P. V. Satyanarayana, N. Veeraiah, *Solid state commun.*, **2010,** *150*, 9-13.

[66] R. S. Manzan, J. P. Donoso, C. J. Magon, I. D. Silva, C. Rüssel, M. Nalin, *J. Braz. Chem. Soc.*, **2015,** *26*, 2607-2614.

[67] A. R. Molla, R. P. S. Chakradhar, C. R. Kesavulu, J. L. Rao, S. K. Biswas, *J. Alloys Compd.* **2012**, *512*, 105-114.

[68] A. F. van Driel,I. S. Nikolaev, P. Vergeer, P. Lodahl, D. Vanmaekelbergh, W. L. Vos, *Phys. Rev.B*; **2007**, 75, 035329.

[69] H. Liu, G. Pan, Z. Yang, Y. Wen, X. Zhang, S. T. Zhang, W. Li, B. Yang, , *Adv. Opt. Mater.,* **2022**, *10*, 2102814.

[70] S.Q. Bai, I.H.K. Wong, *Crystals*, **2018**, *8*, 16.